

Theranostics

2026; 16(4): 1833-1854. doi: 10.7150/thno.120844

Research Paper

Long-acting management of diabetes and associated complications using an injectable thermosensitive hydrogel incorporating IgG-conjugated GLP-1RA

Hancheng Wang¹, Zhiyong Chen¹, Siyi Gu¹, Yaoben Wang¹, Yang Wang¹, Caiyun Gao¹, Jiayue Shi¹, Jiandong Ding¹, Qinghua Wang², Xin Yu¹, □

- 1. State Key Laboratory of Molecular Engineering of Polymers, Department of Macromolecular Science, Fudan University, Shanghai 200438, China.
- 2. Department of Endocrinology and Metabolism, Huashan Hospital, Shanghai Medical School, Fudan University, Shanghai 200040, China.
- 3. Innogen Pharmaceutical Technology Co., Ltd., Shanghai 201203, China.
- Corresponding authors: E-mail address: qh_wang@fudan.edu.cn (Q. Wang) and yu_lin@fudan.edu.cn (L. Yu).

 $\[mathcase]$ The author(s). This is an open access article distributed under the terms of the Creative Commons Attribution License (https://creativecommons.org/licenses/by/4.0/). See https://ivyspring.com/terms for full terms and conditions.

Received: 2025.07.02; Accepted: 2025.10.27; Published: 2026.01.01

Abstract

Rationale: The emergence of glucagon-like peptide-I receptor agonists (GLP-1RAs) has advanced diabetes management. Nevertheless, frequent administration remains a challenge, even with weekly formulations. Herein, we developed a sustained-release hydrogel-based delivery system for Efsubaglutide Alfa (Suba), an IgG-conjugated GLP-1RA, designed to alleviate treatment burden and enhance patient adherence.

Methods: A series of biodegradable poly(lactic acid-co-glycolic acid)-poly(ethylene glycol)-poly(lactic acid-co-glycolic acid) (PLGA-PEG-PLGA) triblock copolymers were synthesized, and a thermosensitive PLGA-PEG-PLGA hydrogel with suitable sol–gel transition temperature and *in vivo* degradation profile was selected for the fabrication of the Suba-loaded hydrogel system (Suba@T-gel). The pharmacokinetic and pharmacodynamic profiles following subcutaneous administration of Suba@T-gel were evaluated in multiple rodent models.

Results: In vivo non-invasive imaging and pharmacokinetic studies showed that a single subcutaneous injection of Suba@T-gel enabled sustained release of Suba for over three weeks. This prolonged release profile is attributed to moderate Suba-polymer interactions and the large molecular size of Suba, which facilitate sustained drug release through a carrier degradation-controlled mechanism. In diabetic murine models, a single administration of Suba@T-gel achieved stable glycemic control for three weeks. Furthermore, the continuous liberation of Suba remarkably enhanced insulin secretion, reduced glycosylated hemoglobin levels, and improved pancreatic function in diabetic mice. Additionally, this system ameliorated diabetes-related complications by improving lipid metabolism, reversing hepatic steatosis and enhancing nerve fiber density.

Conclusions: The Suba@T-gel system represents a promising strategy for long-acting management of diabetes and substantial improvement in patient compliance.

Keywords: type 2 diabetes mellitus; glucagon-like peptide-1 receptor agonists; injectable hydrogel; long-acting formulation; glycemic control

Introduction

Diabetes mellitus, which has emerged as one of the most critical public health challenges of our era, is a chronic endocrine and metabolic disorder characterized by persistent hyperglycemia and a myriad of associated complications, such as cardiovascular disease, neuropathy and nephropathy [1-3]. According to the International Diabetes Federation (IDF), more than 500 million people worldwide are currently afflicted with diabetes, with type 2 diabetes mellitus (T2DM) accounting for over 90% of cases [1, 2, 4]. Most patients with diabetes will develop complications, and cardiovascular complications are the leading cause of diabetes-related mortality [2, 4]. Therefore, achieving adequate glycemic control while effectively managing diabetes complications is the key to extending patients' lives and improving their quality of life. Unfortunately, nearly half of individuals with T2DM

fail to achieve adequate glycemic control, with poor medication adherence—largely due to the burden of frequent invasive injections—being a major contributing factor [5].

Glucagon-like peptide-1 (GLP-1) is an incretin hormone secreted by intestinal L-cells that enhances insulin secretion in a glucose-dependent manner while suppressing glucagon release [6]. Meanwhile, GLP-1 can retard gastric emptying and promote satiety, thereby contributing to weight loss-one of the critical factors in managing T2DM [7, 8]. Additionally, numerous studies have disclosed that GLP-1 expression may bring benefits to multiple organs beyond glucose regulation [7, 9-14]. However, the very short half-life $(t_{1/2})$ of endogenous GLP-1, due to its rapid degradation by dipeptidyl peptidase-4 (DPP-4), limits its therapeutic utility [15]. To surmount this limitation, various GLP-1 receptor agonists (GLP-1RAs) have been exploited through structural modifications to extend their $t_{1/2}$ and thus enhance their duration of action and efficiency in vivo [16-19].

Currently, GLP-1RAs have replaced insulin as the preferred injected antidiabetic drugs for the management of T2DM, as recommended by major international clinical guidelines [20]. Different from earlier generations of GLP-1RAs, such as exenatide, liraglutide and lixisenatide, which administration once or twice daily [21-23], long-acting GLP-1RAs offer superior glycemic control for T2DM management while reducing the burden of frequent injections [17, 24]. Efsubaglutide Alfa (Suba), developed by Innogen Pharmaceutical Technology Co., Ltd., is a novel long-acting GLP-1RA designed to extend in vivo $t_{1/2}$ and dosing intervals while maintaining efficacy. It is a recombinant GLP-1 analog conjugated to the Fc domain of IgG2, which enhances its stability and reduces renal clearance [25, 26]. Preclinical studies have demonstrated its ability to improve glucose homeostasis, pancreatic function, and metabolic health in diabetic rodent and non-human primate models [26, 27]. In clinical trials, Suba has shown robust reductions in glycated hemoglobin (HbA_{1c}), durable glycemic control, and a prolonged $t_{1/2}$ compared to existing GLP-1RAs [17, 24, 27, 28]. In January 2025, it received regulatory approval in China as a once-weekly formulation for blood sugar control in adults with T2DM.

While weekly GLP-1RA formulations improve adherence compared to daily injections, studies suggest that the difference in patient compliance is not as significant as expected [5, 29]. This highlights the urgent need to develop ultra-long-acting formulations that can further reduce injection frequency, such as monthly administration. Unlike

insulin, GLP-1RAs are ideal candidates for sustained-release delivery systems due to their glucose-dependent mechanism, which minimizes hypoglycemia risk [21, 30, 31]. Therefore, further prolonging the duration of GLP-1RAs based on sustained-release carriers holds considerable clinical demand and economic benefits.

Over the past decade, injectable thermosensitive hydrogels comprised of poly(ethylene glycol) (PEG)-polyester [32-36], PEG-polypeptide [37-40], poly(phosphazene)s [41, 42] and other amphiphilic polymers [43-45] have garnered growing attention as promising contenders for sustained drug delivery on account of their good biocompatibility and minimally invasive administration. Generally speaking, these systems are injectable sols at low or room temperatures, facilitating the encapsulation of fragile therapeutic agents such as proteins and peptides through simply mixing. This loading process not only prevents the denaturation/degradation of proteins and peptides but also minimizes drug loss [46, 47]. Once injected into the body, the therapeutic payloads are spontaneously wrapped within the in-situ forming hydrogels as a consequence of the body temperature-triggered sol-gel transition, followed by continuous release of therapeutic agents from the gel depots via drug diffusion or/and carrier polymer degradation.

In this study, we developed a hydrogel-based sustained-release formulation of Suba that alleviates treatment burden by substantially reducing the frequency of injections while maintaining efficacy. Given that OncoGel®, a thermosensitive poly(lactic acid-co-glycolic acid)-poly(ethylene glycol)-poly (lactic acid-co-glycolic acid) (PLGA-PEG-PLGA) polymer hydrogel loaded with paclitaxel was ever approved for Phase IIb clinical trials, this reflects regulatory recognition of the biocompatibility and safety profile of PLGA-PEG-PLGA hydrogels [48, 49]. Therefore, we selected this type of hydrogel as the delivery carrier for Suba. By screening a series of PLGA-PEG-PLGA triblock copolymers with varying PEG/PLGA and lactic acid (LA)/glycolic acid (GA) ratios, a thermosensitive PLGA-PEG-PLGA hydrogel suitable for the sustained release of Suba was confirmed. Subsequently, the interactions between Suba and PLGA-PEG-PLGA polymers investigated, and the sustained release of Suba was detected in vitro and in vivo. The pharmacokinetic profile and therapeutic efficacy sustained-release formulation of Suba were evaluated in four rodent models using multiple observation methods. Finally, its benefits to diseased organs and diabetes-related complications were determined. Overall, this hydrogel-based sustained-release system

has the potential to enable once-monthly dosing, offering a clinically viable and patient-friendly alternative for T2DM management. Figure 1 summarizes the study rationale and objectives.

Results

Synthesis and characterization of PLGA-PEG-PLGA copolymers

A series of PLGA-PEG-PLGA triblock copolymers, designated as Copolymer I to V, with various molecular weights (MWs) and LA/GA ratios were synthesized via a one-step reaction, as depicted in Figure 2A. The compositions and number-average MWs (M_n s) of the synthesized copolymers were determined using their 1 H nuclear magnetic resonance (1 H-NMR) spectra (Figure 2B). Gel permeation chromatography (GPC) analysis further revealed that the synthesized samples exhibited

relatively small molar mass dispersity ($\theta_{\rm m}$) values, signifying that their purity was sufficient to investigate their physicochemical properties. The basic parameters of the resulting copolymers are summarized in Table 1.

Table 1. Basic information of PLGA-PEG-PLGA triblock copolymers in this study.

Sample	M_n (g/mol)(a)	LA/GA (mol/mol) ^(a)	M_w (g/mol) (b)	$D_m(b)$
Copolymer-I	1550-1500-1550	3.3: 1	4700	1.29
Copolymer-II	1840-1500-1840	3.2: 1	5300	1.22
Copolymer-III	2250-1500-2250	3.3: 1	6400	1.28
Copolymer-IV	1890-1500-1890	1.0: 1	5300	1.17
Copolymer-V	1890-1500-1890	9.5: 1	5000	1.20

 $[^]a$ The M_n of PEG block was provided by Sigma-Aldrich. The M_n of PLGA block and the ratio of LA to GA were determined by $^1\text{H-NMR}$ analysis.

^bThe ratio of weight-average MW ($M_{\rm w}$) to $M_{\rm n}$ is defined as $D_{\rm m}$. The $M_{\rm w}$ s and $D_{\rm m}$ values of polymers were obtained by GPC.

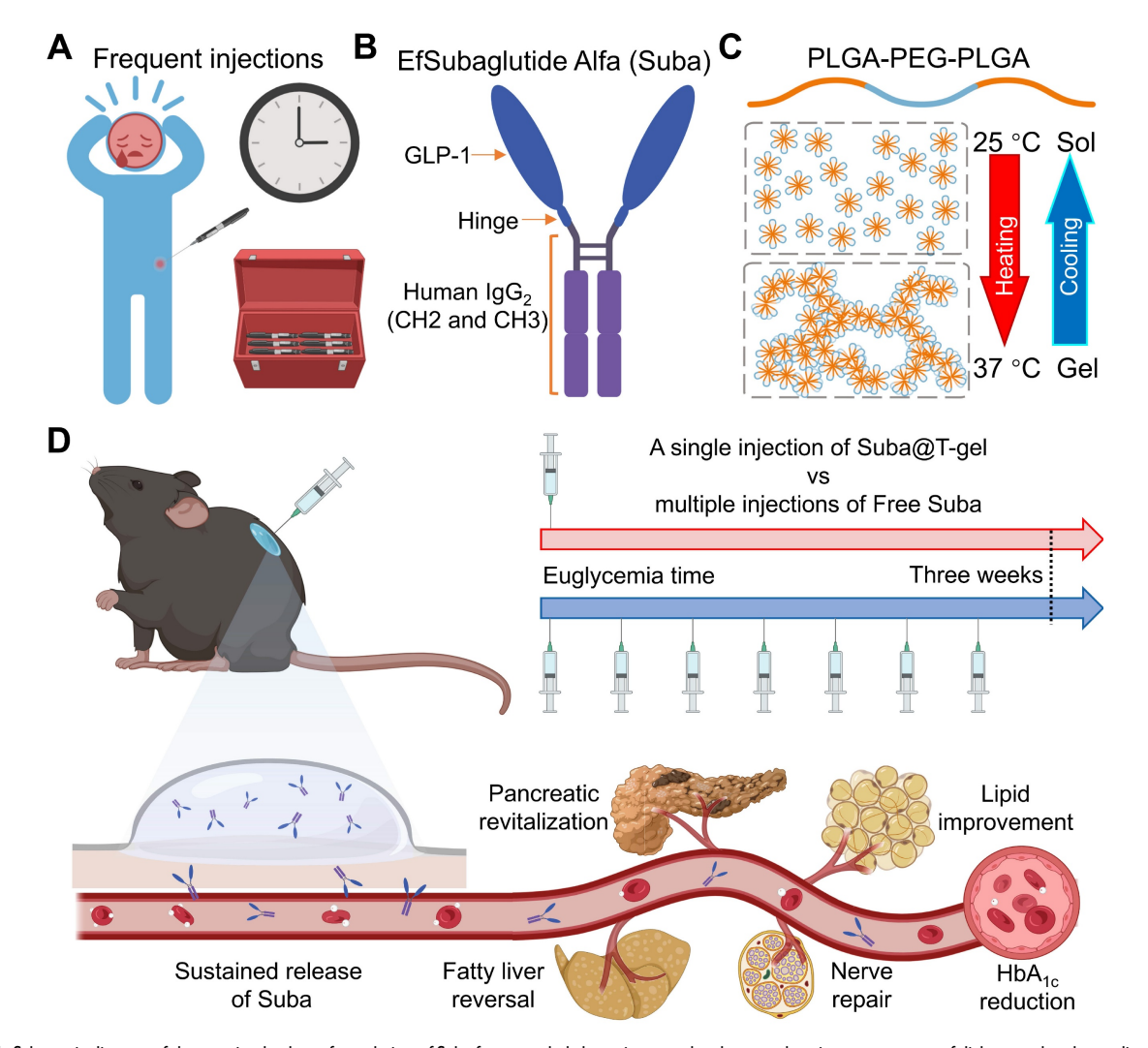


Figure 1. Schematic diagram of the sustained-release formulation of Suba for extended glycemic control and comprehensive management of diabetes-related complications. (A) Conventional frequent injections pose a significant burden on patients and impact adherence. (B) Structural composition of Suba, an IgG-conjugated GLP-1RA. (C) Thermoreversible sol-gel transition feature of PLGA-PEG-PLGA hydrogel. A sol is a suspension of micelles formed by PLGA-PEG-PLGA polymers, while in the gel state, a percolated network is created through micellar aggregation. (D) A single administration of the sustained-release formulation of Suba achieves prolonged glycemic control for three weeks in diabetic mice and effectively ameliorates multiple diabetes-related complications, including dyslipidemia, fatty liver, and neuropathy.

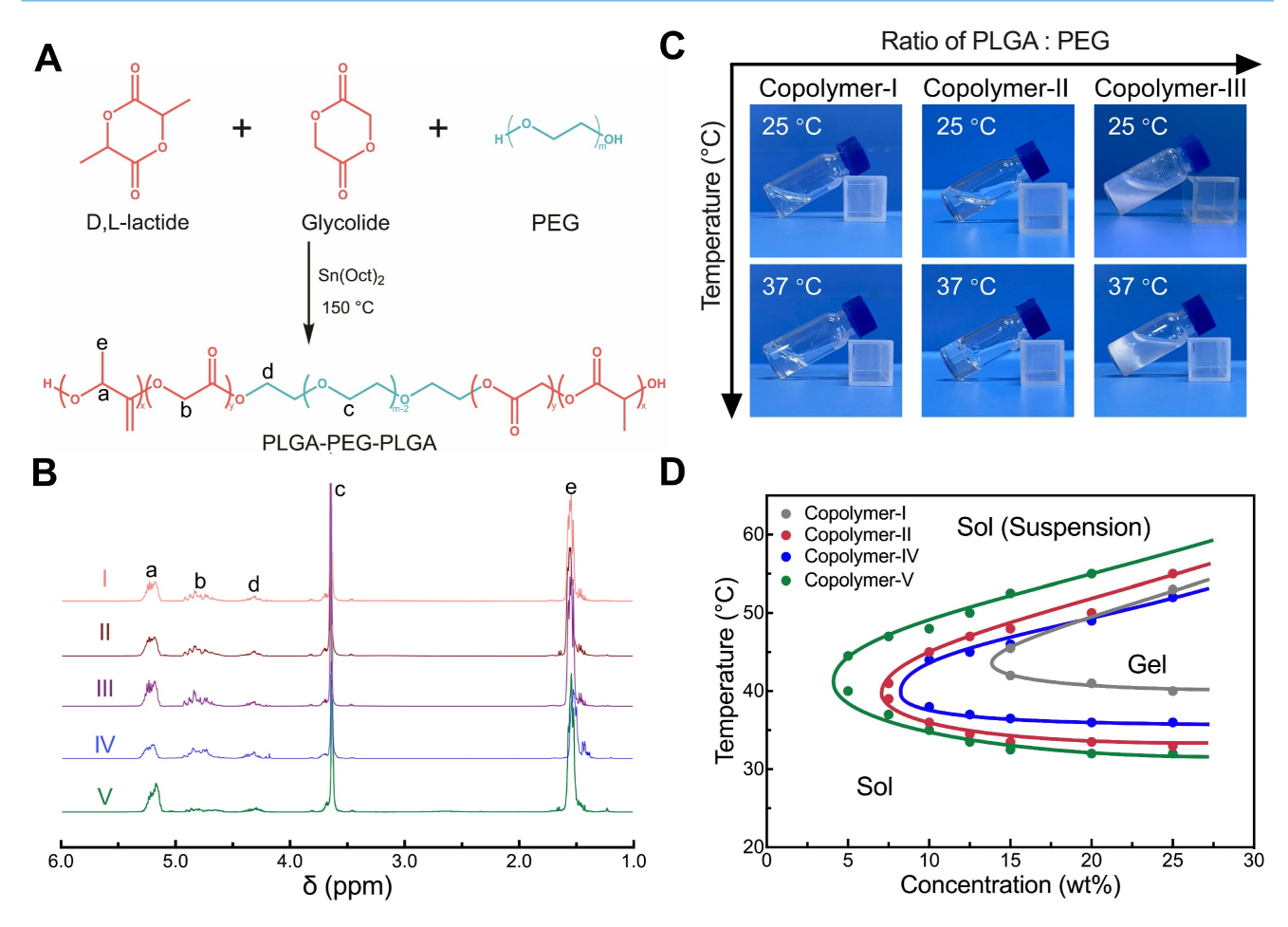


Figure 2. Synthesis of PLGA-PEG-PLGA and characterization of the hydrogels. (A) Synthesis route of PLGA-PEG-PLGA. (B) ¹H-NMR spectra of PLGA-PEG-PLGA triblock copolymers with different MWs and segment ratios. (C) Optical images of different copolymer/water systems at room temperature or body temperature. (D) Phase diagrams of different copolymer/water systems illustrating the sol-gel transition at varying concentrations and temperatures.

Temperature-responsive sol-gel transition of aqueous polymer solutions

the synthesized copolymers, Among Copolymer-III, containing the longest PLGA block, was overly hydrophobic and failed to dissolve in water, making it unsuitable for further investigation. The remaining four PLGA-PEG-PLGA copolymers exhibited solubility in water and spontaneously underwent sol-gel transitions with increasing (Figure 2C-D). temperature Among them, Copolymer-I remained in a sol state at body temperature, suggesting its inappropriateness for in *vivo* applications. In contrast, the other three systems (Copolymer-II, IV, and V) formed semi-solid hydrogels at body temperature, indicating their potential as drug delivery carriers. Notably, despite having comparable MWs, their gelation windows and gel strengths were influenced by the LA/GA ratio in the PLGA block. A higher proportion of LA units resulted in a lower sol-gel transition temperature (T_{gel}) , a wider gelation window and an increased gel modulus (Figure 2D and S1).

Biocompatibility and biodegradation of thermosensitive hydrogels

We explored the *in vivo* persistence of thermosensitive hydrogels composed of 25 wt% aqueous solutions of Copolymer-II, IV, and V in Institute of Cancer Research (ICR) mice. Figure 3A illustrates the injection sites of the hydrogel and the subsequent assessment methods. It was evident that the *in vivo* maintenance of PLGA-PEG-PLGA hydrogel was also contingent on the LA/GA ratio, and a higher proportion of LA units correlated with a slower degradation *in vivo* (Figure 3B). Given that the thermosensitive hydrogel composed of Copolymer-II, denoted as T-gel in this study, had the most suitable degradation period, approximately one month, this system was chosen as the delivery carrier of Suba for following experiments.

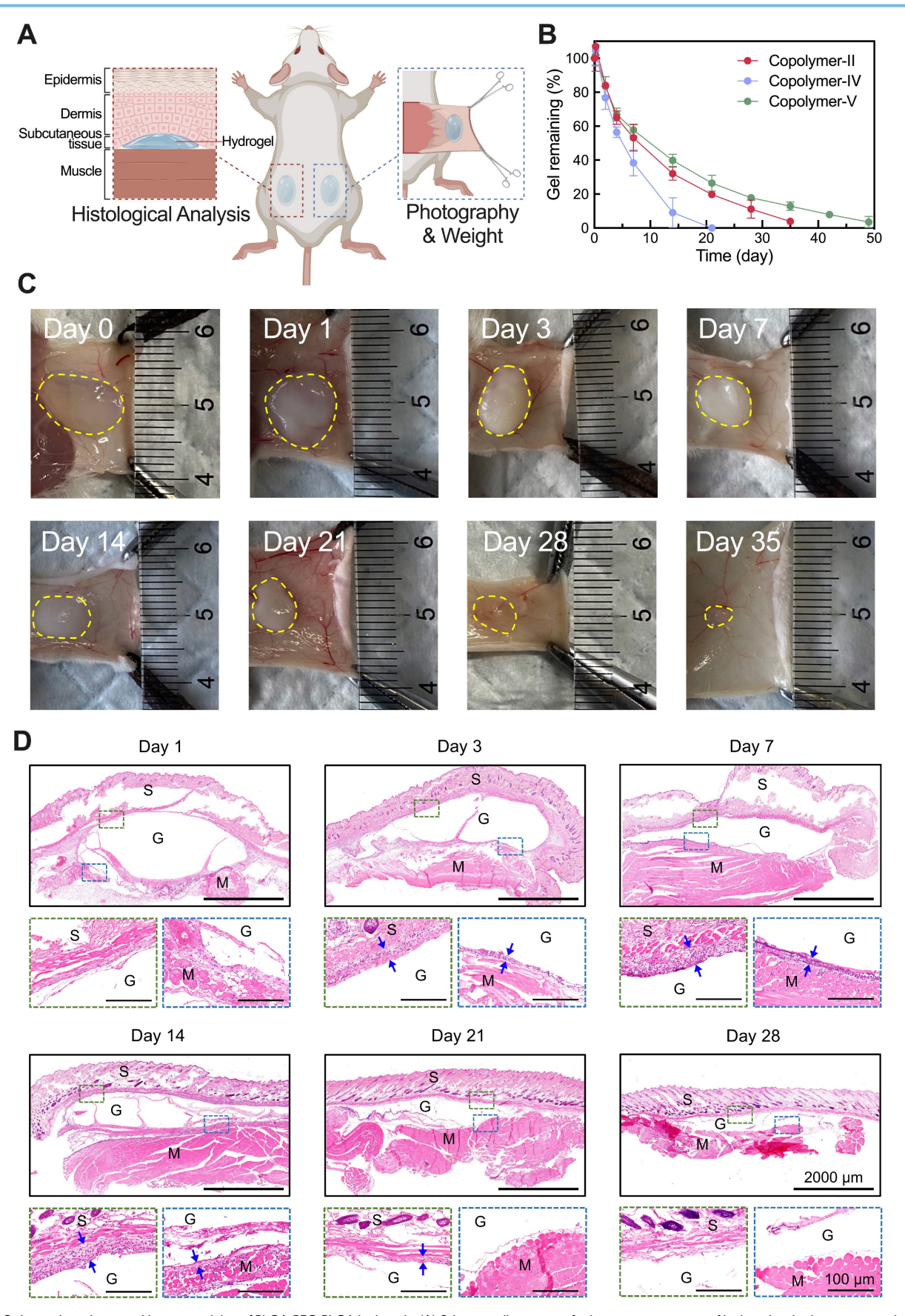


Figure 3. In vivo degradation and biocompatibility of PLGA-PEG-PLGA hydrogels. (A) Schematic illustration of subcutaneous injection of hydrogel and subsequent sampling and analysis. (B) Degradation profiles showing changes in the remaining mass of injected hydrogels over time (n = 4). (C) Optical images of residual T-gel at indicated time points. The yellow dashed lines delineate the contour of the residual gel. (D) H&E-stained sections of tissues containing residual T-gel at indicated time points. S: skin, M: muscle, and G: residual gel. The blue arrows denote the generated fibrous layer, which is barely observable on day 28.

Figure 3C portrays the changes in morphology and size of the residual T-gel as a function of degradation time. The hydrogel initially exhibited a transparent state following subcutaneous injection, and then transformed into an opaque state. This change may be ascribed to the erosion of its hydrophilic components [50]. Meanwhile, hydrogel's volume gradually decreased with the effluxion of time. To further monitor the compositional changes of T-gel during degradation, the gel residues collected at predetermined time points were freeze-dried and subjected to ¹H NMR analysis (Figure S2A). As summarized in Figure S2B, the hydrophilic EG fraction progressively decreased, whereas the hydrophobic LA fraction steadily increased. The GA fraction showed no significant change, likely due to its relatively low initial content. These findings indicate continuous degradation of PLGA-PEG-PLGA polymers and faster absorption of hydrophilic degradation products compared to their hydrophobic counterparts. In addition, our previous study has demonstrated that the degradation products of PLGA-PEG-PLGA polymers are primarily eliminated through the liver, gallbladder, and spleen [50].

Gross anatomical examination of the injection region revealed no signs of edema, necrosis, or suppuration. Subsequently, some residual gels containing surrounding tissues were also harvested for histological analysis, and the results showed a mild inflammatory response at the implantation site, which diminished as the hydrogel degraded (Figure 3D). Additionally, cell counting kit-8 (CCK-8) assay demonstrated that even at concentrations as high as 1000 μg/mL, Copolymer-II did not exhibit significant cytotoxicity against fibroblasts, adipocytes, or islet cells (Figure S3). These findings, combined with its low hemolysis rate (Figure S4) and normal blood routine index of mice after injection (Figure S5), collectively validated its suitability as a drug delivery vehicle.

Preparation and characterization of the sustained-release Suba formulation (Suba@T-gel)

T-gel was a low-viscous sol at room temperature, which facilitated the encapsulation of Suba through simple physical mixing, thereby forming the sustained-release formulation Suba@T-gel. As displayed in Figure 4A, Suba@T-gel containing 2.5 mg/mL Suba maintained its sol state at room temperature and converted into a non-flowing gel at physiological temperature; the introduction of Suba reduced the transparency of Suba@T-gel compared with the Suba-free T-gel system. Dynamic rheological

measurements further demonstrated that the incorporation of Suba resulted in a reduction in the $T_{\rm gel}$ of Suba@T-gel by approximately three degrees relative to the Suba-free T-gel system, but did not obviously affect its modulus (Figure 4B).

mechanism of temperature-response gelation of PEG-polyester copolymer hydrogels arises from the aggregation of micelles self-assembled by these PEG-polyester copolymers in water, which form a percolated micellar network upon heating [46, 51-54]. Dynamic light scattering (DLS) analysis (Figure 4C) and transmission electron microscopy (TEM) observations (Figure 4D) confirmed that the T-gel system follows the same gelation mechanism. We further found that the introduction of Suba did not influence the critical micelle concentration (CMC) of Copolymer-II in water (Figure S6), whereas the micelles incorporating with Suba exhibited an increased size and tended to aggregate at lower temperatures (Figure 4C-D). Obviously, the earlier aggregation of micelles led to a decrease in the $T_{\rm gel}$ of Suba@T-gel.

To further explore the possible interactions between the drug and the carrier, circular dichroism (CD) analysis of Suba with or without the carrier polymer was conducted. Pure Suba predominantly exhibited an α-helix structure (Table S1 and Figure 4E). A red shift of CD signal was noticed upon the addition of Copolymer-II, indicating a significant reduction in the α -helix content accompanied by an increase in random coil structures, as shown in Figure 4E. Such structural changes were not observed when Suba was mixed with PEG or replaced by BSA (Figure 4E and S7A). Computational simulation of Suba's amino acid sequence revealed the presence of alternating hydrophilic and hydrophobic regions within Suba (Figure S7B). Consequently, we speculate participated amphiphilic Suba self-assembly process of Copolymer-II in water, leading to an increased micelle size and promoting the formation of the hydrogel network.

The robust stability of Suba was also confirmed. As shown in Figure S8, neither secondary structure changes nor degradation were detected even when a Suba solution was incubated in a water bath shaker at 37 °C for five days. This stability was significantly superior to other GLP-RAs such as exenatide [55].

Subsequently, the *in vitro* release profile of Suba@T-gel was evaluated while employing F127-gel and poly(vinyl alcohol) (PVA)-gel as the controls (Figure S9). The PVA-gel used in this study was fabricated by the classic freeze-thaw method and is well established as a non-degradable hydrogel [56, 57]. As illustrated in Figure 4F, Suba experienced a rapid release from F127-gel following the rapid

dissolution of the gel matrix in the release medium (Figure S10A). Conversely, due to the high stability of its structural integrity (Figure S10B), Suba exhibited a very slow and incomplete release from PVA-gel, with only 40% of the drug released within 60 days. Unlike the F127-gel and PVA-gel systems, Suba@T-gel displayed a sustained release pattern for up to 60 days

without a significant burst release at the first stage or severe incomplete release at the late stage (Figure 4F). Additionally, it should be noted that different from biodegradable T-gel, the non-degradable PVA-gel exhibits considerable risks of polymer accumulation *in vivo* after repeated administration.

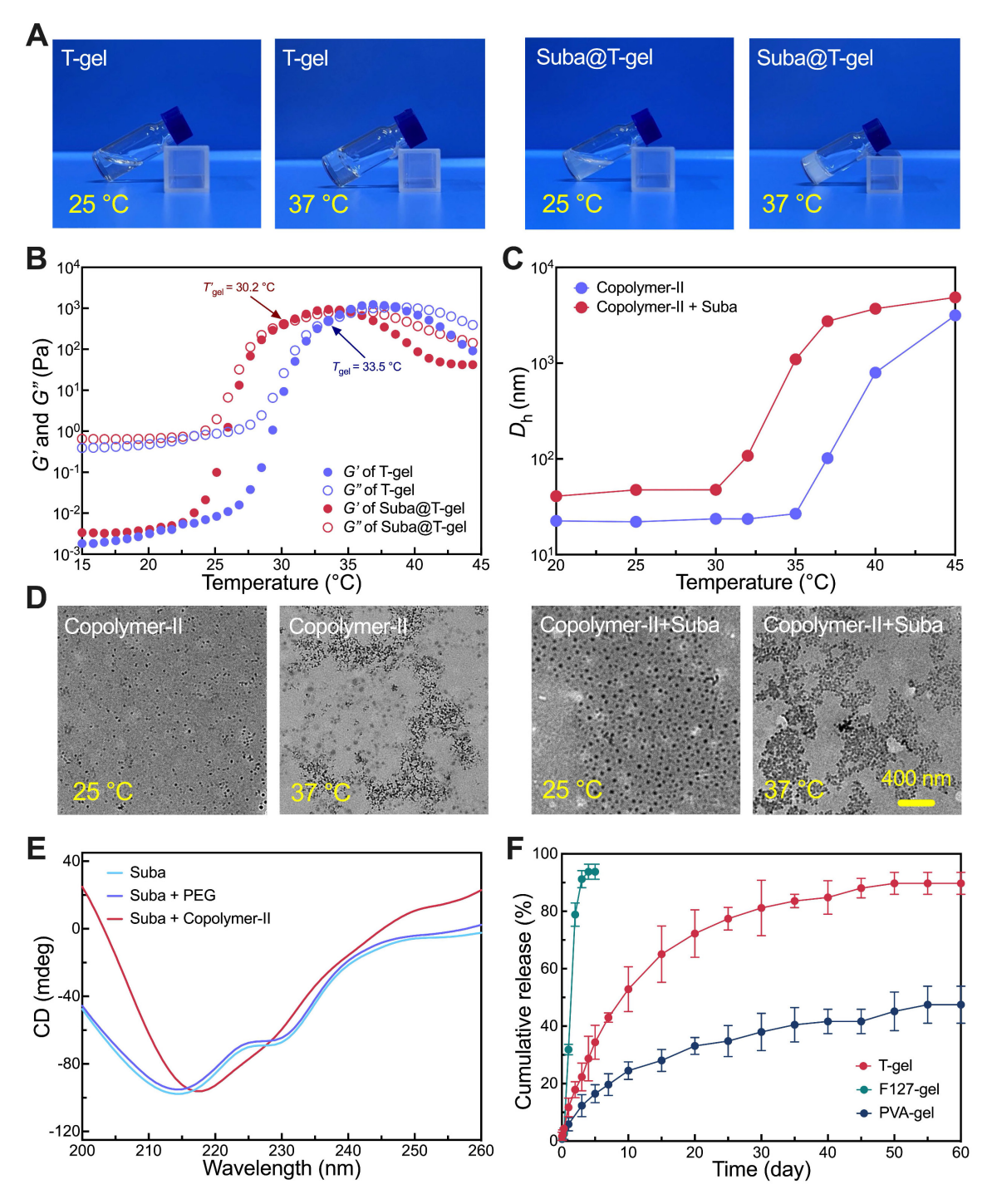


Figure 4. Characterization of Suba@T-gel. (A) Optical images of T-gel and Suba@T-gel at two indicated temperatures. (B) Rheological curves of T-gel and Suba@T-gel as a function of temperature. (C) Hydrodynamic size of Copolymer-II micelles in water with or without Suba at different temperatures. (D) TEM images of micelles formed by Copolymer-II with or without Suba at two indicated temperatures. (E) CD spectra assessing the structural integrity of Suba with and without PEG/Copolymer-II. (F) In vitro release profiles of Suba from different hydrogel formulations (n = 3).

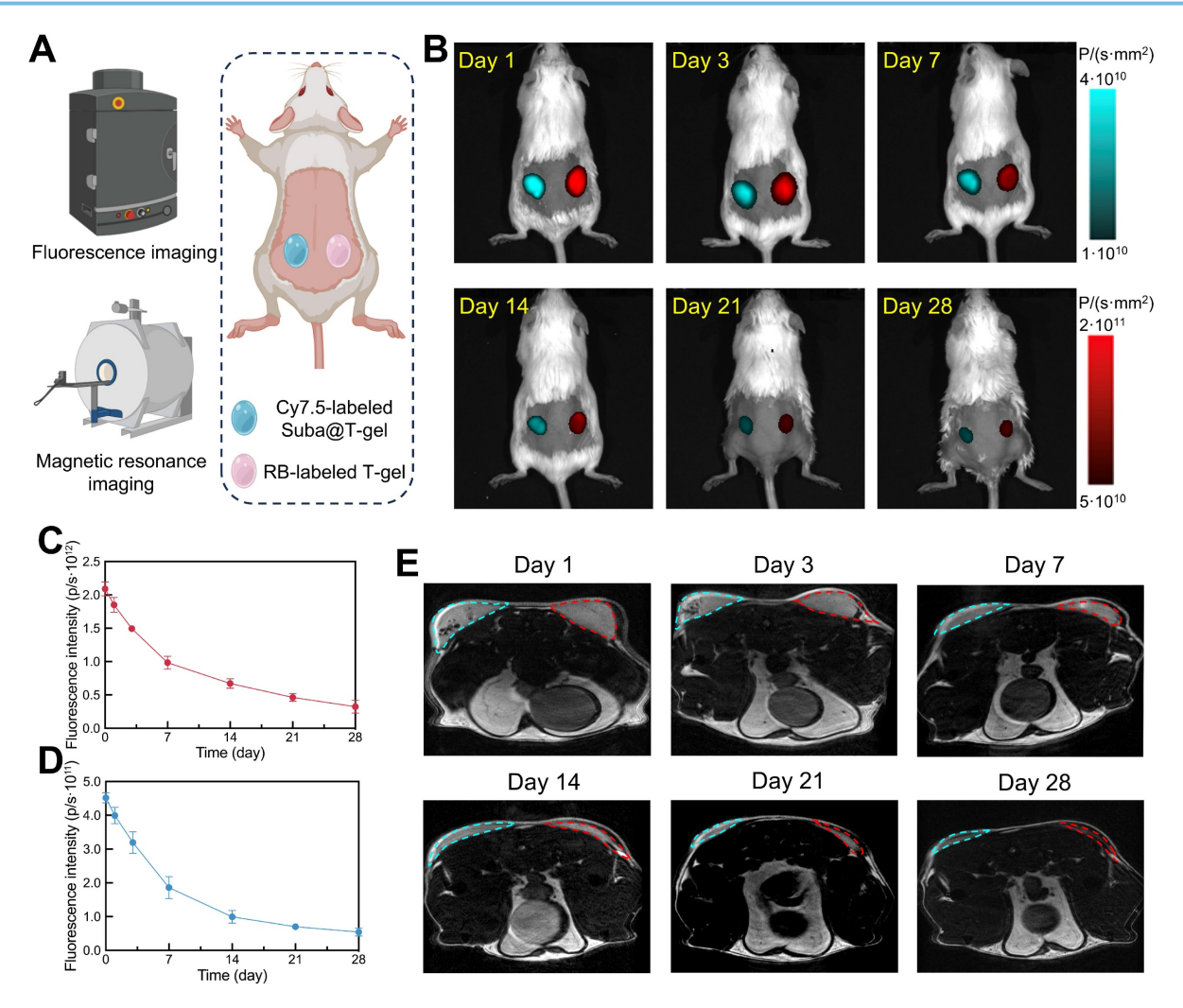


Figure 5. Non-invasive tracing of Suba@T-gel in vivo. (A) Schematic illustration of non-invasive monitoring of subcutaneously injected Suba@T-gel and T-gel using fluorescence imaging and MRI. (B) Representative fluorescence images of mice at indicated time points after injection of Suba@T-gel and T-gel. The data was obtained from the same mouse. (C, D) Changes in total fluorescence intensity of RB-labled T-gel (C) and (D) Cy7.5-labled Suba@T-gel as a function of time (n = 3). (E) Representative MRI images of mice at indicated time points after injection of Suba@T-gel and T-gel. The cyan dashed lines indicate the contour of Suba@T-gel, while the red dashed lines represent the outline of T-gel. The data was obtained from the same mouse.

Determination of the optimal drug-loading amount in Suba@T-gel

The oral glucose tolerance test (OGTT) in normal ICR mice is a cost-effective model for evaluating formulation efficacy [58]. Therefore, we conducted OGTTs in normal ICR mice to confirm the optimal Suba loading concentration in Suba@T-gel. As illustrated in Figure S11, oral administration of glucose led to a rapid increase in blood glucose levels in the placebo group, whereas the administration of Suba@T-gel at different drug concentrations significantly attenuated postprandial glucose excursions during their respective effective periods. The 2.5 mg/mL formulation maintained glycemic control for up to 22 days, demonstrating a long-lasting hypoglycemic effect (Figure S11). In comparison, the 1.25 mg/mL formulation achieved glycemic control only until day 18, while the 5 mg/mL formulation did

not provide an extended duration of control relative to the 2.5 mg/mL dose. Notably, at the 5 mg/mL dose, a few mice exhibited fasting hypoglycemia during the initial phase of administration, suggesting a potential risk of side effects associated with excessive dosing. In contrast, no hypoglycemic symptoms were observed in the 2.5 mg/mL group throughout the study period. These findings support the 2.5 mg/mL formulation as the optimal dosage of Suba@T-gel for sustained glycemic control. Therefore, in all subsequent experiments, the Suba dose in Suba@T-gel was fixed at 2.5 mg/mL.

Non-invasive monitoring of Suba@T-gel in vivo

To visualize *in vivo* Suba release, non-invasive fluorescence imaging and magnetic resonance imaging (MRI) were employed. Cy7.5-modified Suba was introduced into Suba@T-gel, while rhodamine B (RB)-capped Copolymer-II as a macromolecular

fluorescent probe was incorporated into T-gel. The two systems were injected separately into the left and right sides of the ICR mice's back, as illustrated in Figure 5A. As shown in Figure 5B, the drug or carrier containing fluorescent moieties could be distinctly visualized in the subcutaneous region of the mice. Meanwhile, as the hydrogel degraded or the drug was released, the fluorescence signal intensity gradually diminished. The change trend of total fluorescence intensity for Suba was consistent with that of the carrier polymer (Figure 5C-D), indicating that the degradation of T-gel governed the release of Suba. After approximately three weeks of release, the fluorescence signal of Suba dropped to a very low These findings provide an intuitive level. understanding of in vivo Suba release.

MRI is an efficacious approach for observing materials/tissues with high water content, such as hydrogels and cartilage, especially when utilizing T_2 -weighted sequences [50, 59]. This technique enabled us to clearly visualize the changes in volume and signal intensity of hydrogels over time. As shown in Figure 5E, a gradual reduction in hydrogel volume over time was clearly observed, and the signal intensity decreased significantly about three weeks post-injection, with the hydrogel boundaries becoming indistinguishable after four weeks. Comparisons of transverse plane images between hydrogels with and without Suba showed that the addition of Suba appeared to contribute to water retention within the hydrogel matrix (Figure 5E).

Pharmacokinetic assessment

Pharmacokinetic studies were further performed in Sprague-Dawley (SD) rats to evaluate the maintenance of effective therapeutic concentrations following a single injection of the optimized Suba@T-gel formulation (2.5 mg/mL) (Figure 6). The pharmacokinetic parameters are summarized in Table 2. After a single intravenous administration of Free Suba, plasma drug concentration reached its peak instantaneously and then declined rapidly. In contrast, the time to reach the maximum plasma concentration (T_{max}) was significantly extended in the subcutaneously administered Free Suba@T-gel groups. Meanwhile, the maximum plasma concentration (C_{max}) —a parameter closely associated with the onset of most adverse reactions, particularly gastrointestinal discomfort during the initiation phase [19], was markedly reduced in the Suba@T-gel group, being only approximately half of that observed in the Free Suba (s.c.) group. Furthermore, the $t_{1/2}$ of Suba in the Suba@T-gel group was significantly longer compared to subcutaneously

injected Free Suba. More importantly, a stable plasma concentration of Suba remained above the minimum effective threshold for over 22 days, which was in good agreement with the results of OGTTs (Figure S11).

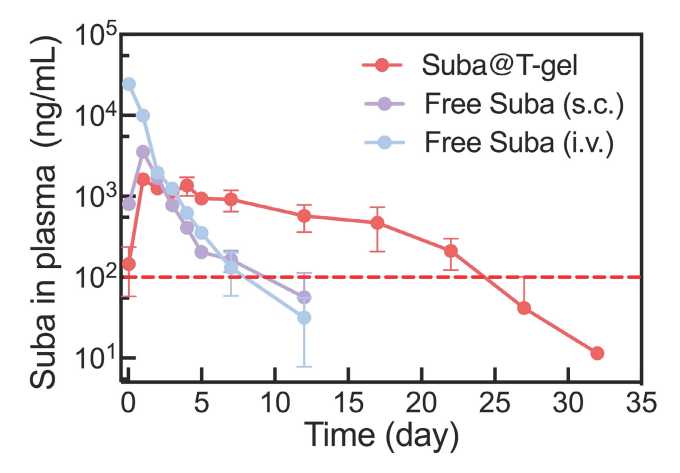


Figure 6. Plasma Suba concentration profiles following a single injection of various Suba formulations in SD rats (n=3). The same dosage of Suba (2.5 mg/kg) was administrated in the three groups. The red dashed line indicates the minimum effective plasma concentration threshold of Suba. S.c.: subcutaneous injection, and i.v.: intravenous injection.

Table 2. Pharmacokinetic parameters of different Suba formulations after a single injection.

	Free Suba (i.v.)	Free Suba (s.c.)	Suba@T-gel
T_{max} (h)	1	24	24
C _{max} (ng/mL)	24410	3546	1700
t _{1/2} (h)	44.9	48.8	76.9
AUC _(0-last) (h ng/mL) ^a	657241	186339	398068
MRT (h)b	23.8	22.4	209.4

 $^a AUC_{(0\text{-}last)};$ area under the curve from time zero to the last sampling time point. $^b MRT;$ mean retention time.

In vivo long-term hypoglycemic effect

We employed a T2DM db/db mouse model to comprehensively investigate the in vivo therapeutic effect of Suba@T-gel. As shown in Figure 7A, the mice in the Suba@T-gel group received only a single injection. Notably, a single subcutaneous administration of Free Suba maintained stable glycemic control in db/db mice for only three days (Figure S12). To achieve sustained and stable glucose regulation, Free Suba was administered every three days, consistent with our previous work [26], and the mice in the Free Suba group received a total of seven injections, with the cumulative dosage equivalent to that of a single dose of Suba@T-gel. During the 22-day experiment period, the placebo-treated mice consistently presented high fasting blood glucose levels (Figure 7B). Conversely, the single injection of Suba@T-gel achieved sustained blood sugar control, with fasting blood glucose levels remaining within the normal range until day 21, which was comparable to the effect of seven injections of Free Suba. The statistical analysis of the blood glucose area under the curve (AUC) further supported the above findings (Figure 7C). In addition, these results indicate that biologically active Suba is released from T-gel.

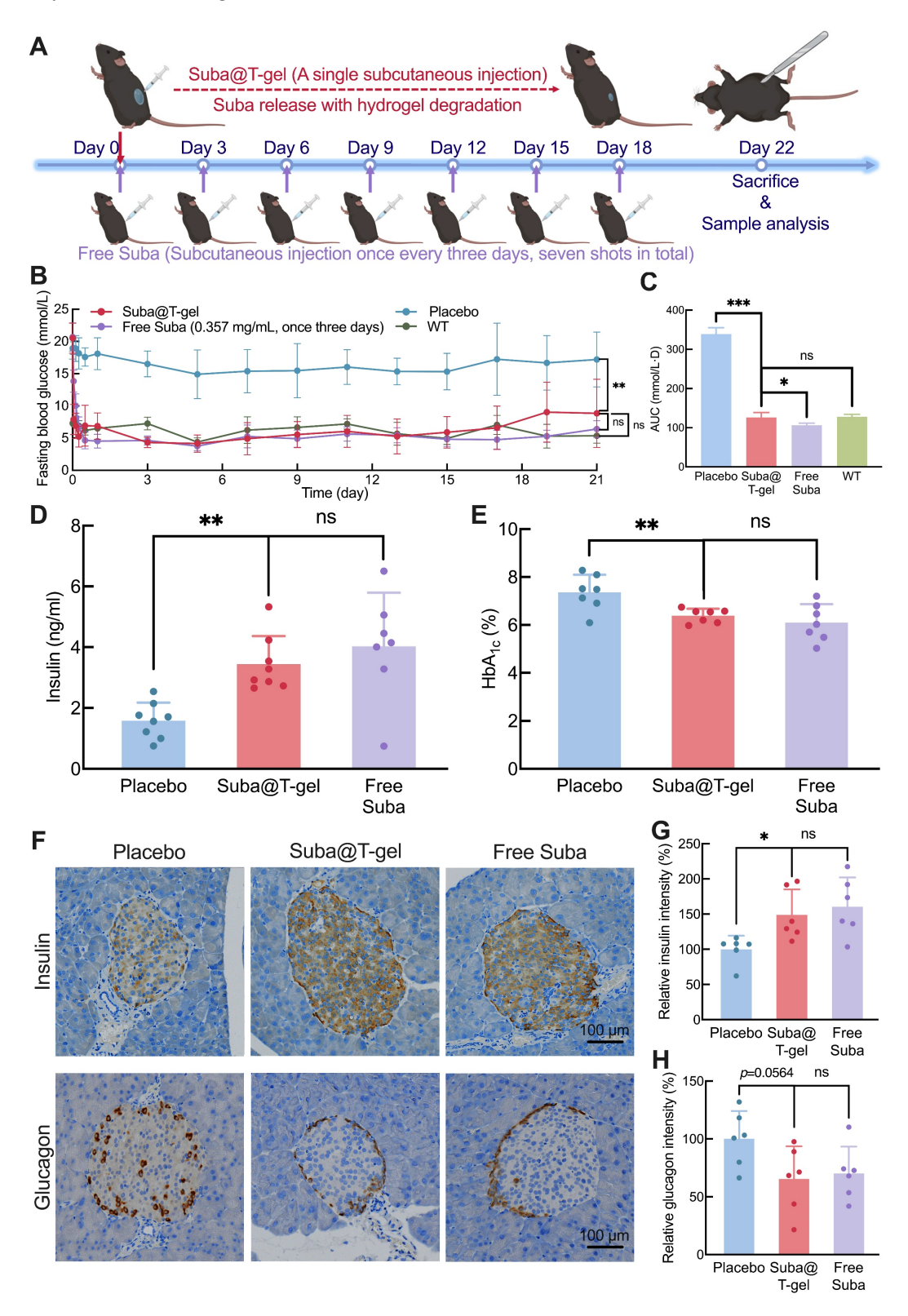


Figure 7. Therapeutic effects of Suba@T-gel in a db/db mouse model. (A) Schematic diagram and timeline of a treatment cycle. (B) Changes in fasting blood glucose levels of mice following different treatments (n = 8). (C) AUC of fasting blood glucose levels after different treatments (n = 8). (D, E) Plasma insulin concentrations and HbA_{1c} levels of mice at the end of various treatments (n = 7-8). (F) Immunohistochemical stained slices of pancreatic tissues at the end of various treatments. (G, H) Quantification of insulin (G) and glucagon (H) immunostaining in pancreatic tissues (n = 6).

In addition, we carried out OGTTs to evaluate postprandial blood glucose levels in db/db mice. The results showed that, even on day 17, the Suba@T-gel group could significantly inhibit the rise in postprandial blood glucose levels (Figure S13). These findings indicate that Suba@T-gel has the potential to serve as a long-acting formulation for the treatment of diabetes, which not only provides stable control of blood glucose levels but also minimizes the injection frequency.

Effects of endocrine mediation and islet repair

Given the important increase in random blood sugar levels (> 18.7 mmol/L) three weeks after a single injection of the Suba@T-gel system (Figure S14), all animals were euthanized on Day 22, and blood samples were collected for further analysis. As displayed in Figure 7D, the plasma insulin concentrations in the Suba@T-gel group were significantly higher than those in the placebo group, indicating that the sustained and steady release of Suba effectively promoted insulin secretion. This effect was comparable to that observed in the mice receiving frequent injections of Free Suba. HbA_{1c}, formed through an irreversible glycosylation reaction, is recognized as the gold standard for long-term glycemic control and can predict the progression of diabetic symptoms [60]. In comparison with the placebo group, both treatments with Suba@T-gel and Free Suba resulted in a significant reduction in HbA_{1c} levels (Figure 7E), with no notable difference between them, suggesting that long-term glycemic control was achieved with a single injection of Suba@T-gel.

Generally, db/db mice exhibit compensatory islet hypertrophy, but in severe cases, β -cell apoptosis occurs, leading to diminished insulin secretion [26, 61, 62]. Immunohistochemical analysis of islet tissues revealed that a single injection of Suba@T-gel significantly enhanced insulin secretion while decreasing glucagon release (Figure 7F-H), akin to the Free Suba group. These results imply that the administration of Suba@T-gel contributes to the repair of β cells, thus improving islet function.

To further validate whether Suba@T-gel can delay the progression of diabetes resulting from insulin deficiency, we employed another mouse model of islet damage induced by streptozotocin (STZ), which more closely resembles type 1 diabetes. Following five consecutive days of intraperitoneal injection of STZ, the mice exhibited a consistent rise in random blood glucose levels, indicating successful modeling (Figure 8A-B). By the fourth week, treatment with a single injection of Suba@T-gel or Free Suba (2.5 mg/mL) was initiated in a subset of mice. The results presented in Figure 8B showed a

significant reduction in blood glucose levels in the STZ + Suba@T-gel group, approaching those of normal mice (the vehicle group). Although blood glucose levels gradually increased over time, they remained significantly lower than those of untreated mice (the STZ group). In contrast, although a single injection of Free Suba led to an initial rapid decrease in blood glucose levels in mice, its efficacy in glycemic control diminished quickly over time. Two weeks after injection, the blood glucose levels in the STZ + Free Suba group were already significantly higher than those in the STZ + Suba@T-gel group. By four weeks, the blood glucose levels in the STZ + Free Suba group had risen to the levels nearly indistinguishable from those in the untreated STZ group.

An OGTT conducted at week 8 further confirmed that both fasting and postprandial glucose levels were lower in the mice treated by Suba@T-gel compared to those in the STZ and STZ + Free Suba groups (Figure 8E).

Subsequently, fluorescence double-label staining of mouse islets revealed that Suba@T-gel treatment promoted β -cell proliferation, as evidenced by the presence of Ki67-positive cells, and enhanced insulin secretion (Figure 8C). Statistical analysis of Ki67 expression and β -cell mass further confirmed that treatment with Suba@T-gel significantly restored islet function (Figure 8F-G), whose effect was markedly superior to that in the STZ + Free Suba group. Additionally, untreated mice and those treated with Free Suba exhibited strong terminal deoxynucleotidyl transferase dUTP nick end labeling (TUNEL) signals, indicative of significant islet apoptosis (Figure 8D). In contrast, TUNEL signals were markedly weaker in the STZ + Suba@T-gel group, confirming that this treatment effectively prevented β-cell apoptosis and preserved islet integrity. These favorable results collectively demonstrate that a single administration of Suba@T-gel, at the same dosage, enables sustained release of Suba, which can more effectively and sustainably prevent chronic pancreatic islet damage compared to a single injection of Free Suba. Taken together, Suba@T-gel not only achieves sustained glycemic control but also promotes the repair and regeneration of islet cells, thereby presenting a promising therapeutic option for diabetes.

Effects on metabolic health and diabetic complications

Considering the intricate and close relationship between obesity and diabetes [2, 4, 63], we also monitored the weight changes in db/db mice undergoing various treatments. It was evident that the treatment of Suba@T-gel effectively postponed weight gain in mice compared with the placebo group

(Figure 9A), although this effect was slightly inferior to that observed in the Free Suba group. Meanwhile, several abrupt fluctuations in body weight were observed in the Free Suba group, which coincided with the dosing time points. Combined with the pharmacokinetic data showing higher plasma Suba concentrations shortly after the injection of Free Suba

(Figure 6), we speculate that the greater body weight reduction is attributable to the higher GLP-1RA exposure, which is consistent with the previous finding [19]. Additionally, both Suba@T-gel and Free Suba treatments significantly decelerated the proportion of muscle loss and the proportion of fat gain in mice relative to the placebo group (Figure 9B).

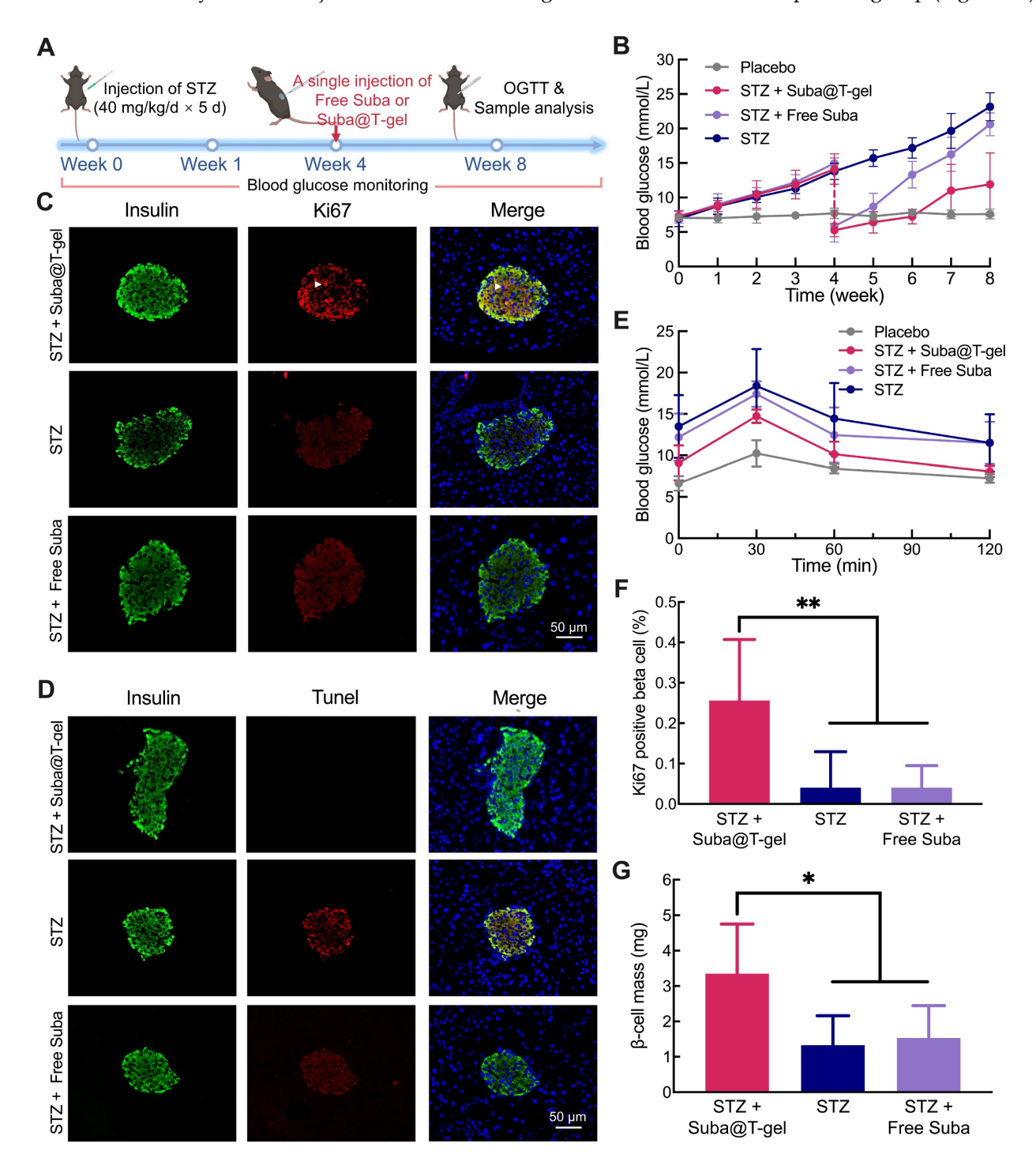


Figure 8. Effects of Suba@T-gel treatment on proliferation of islet cells in STZ-induced diabetic mice. (A) Experimental procedure and timeline. (B) Changes in blood glucose levels after various interventions (n = 8). (C) Insulin (Green) and Ki67 (Red) double stained images of islet cells at the end of various treatments. The white arrows indicate the cell nuclei that are positive for both Ki67 and DAPI staining. (D) Insulin (Green) and Tunel (Red) double stained images of islet cells at the end of various treatments. (E) OGTT results after a single injection of Suba@T-Gel over 4 weeks (n = 8). (F) Quantification of Ki67-positive proliferating cells (n = 6). (G) β -cell mass calculated based on insulin fluorescence staining and islet weight (n = 6).

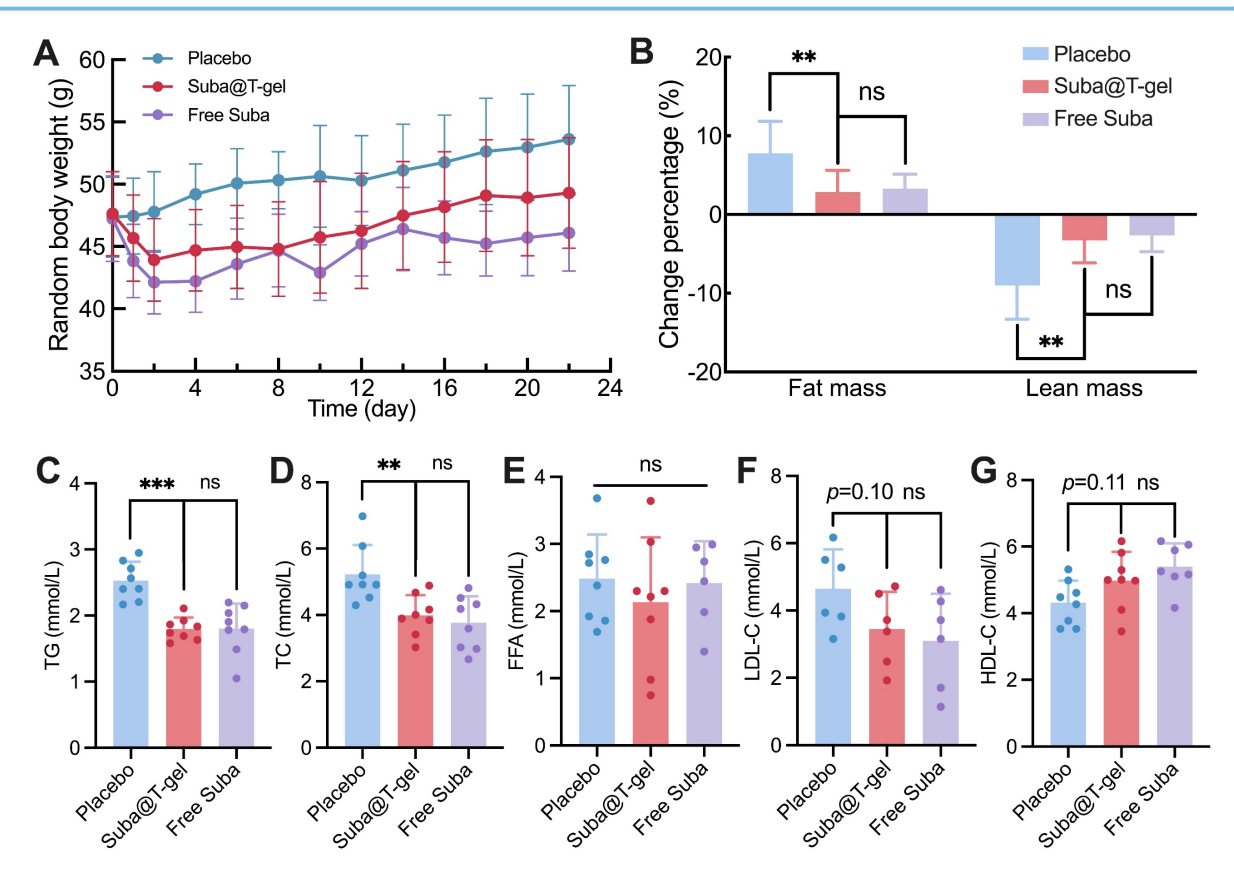


Figure 9. Effects of Suba@T-gel on obesity control and lipid metabolism improvement. (A) Changes in body weight of mice after various treatments (n = 8). (B) Changes in body composition proportions of mice after various treatments (n = 8). (C-G) Serum lipid levels of mice at the end of various treatments: (C) TG, (D) TC, (E) FFA, (F) LDL-C and (G) HDL-C (n = 6-8).

The levels of lipid metabolism markers in blood samples collected on day 22 were detected. Treatment with Suba@T-gel resulted in significant reductions in triglyceride (TG) and total cholesterol (TC) levels, achieving decreases comparable to those seen in the Free Suba group (Figure 9C-D). However, it is noteworthy that serum free fatty acid (FFA) levels remained unchanged regardless of treatment with Suba@T-gel or Free Suba (Figure 9E). High-density lipoprotein cholesterol (HDL-C) is known as a good cholesterol that facilitates the removal of cholesterol from the arterial walls to the liver, whereas low-density lipoprotein cholesterol (LDL-C) is regarded as the "bad" cholesterol because it can cause fatty buildups in the arteries [64, 65]. Although no statistically significant difference was noted compared with the placebo group, a slight increase in HDL-C levels and a decrease in LDL-C levels were observed following a single injection of Suba@T-gel (Figure 9F-G).

Metabolic cages were also utilized to visually assess the metabolic alterations in mice (Figure S15A), primarily taking into account that diabetes patients

often exhibit abnormal excretion patterns such as polyuria [66]. As shown in Figure S15B-C, the administration of Suba@T-gel or Free Suba resulted in a reduction of urine and feces excretion compared with the placebo group. The effect of reduced excretion induced by Suba@T-gel were slightly inferior to that observed in the Free Suba group, which was consistent with the results of weight changes in mice. These findings were further corroborated by AUC calculations (Figure S15B-C).

The progression of diabetes often leads to various complications [2, 4, 60]. After the db/db mice were sacrificed on day 22, systematical anatomical observations were performed. As shown in Figure 10A, Suba@T-gel treatment markedly reduced liver mass in mice, although they did not completely restore to a normal level. Meanwhile, the livers of untreated mice appeared yellowish-white with a rough, nodular surface, indicative of a fatty liver. In contrast, the livers of mice treated with Suba@T-gel or Free Suba exhibited a healthy brownish-red color with a smooth surface, resembling that of normal mice.

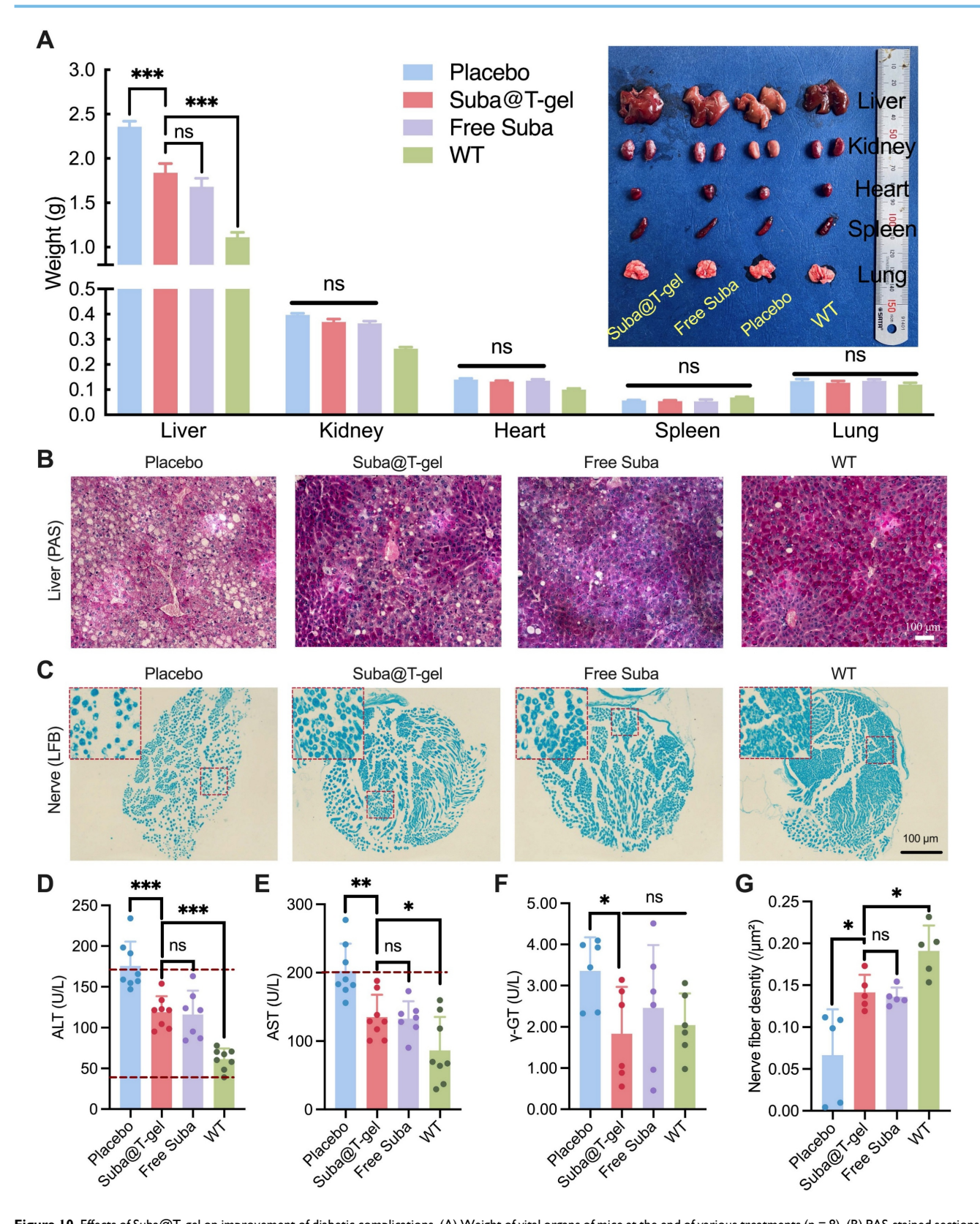


Figure 10. Effects of Suba@T-gel on improvement of diabetic complications. (A) Weight of vital organs of mice at the end of various treatments (n = 8). (B) PAS-stained sections of livers of mice. (C) LFB-stained sections of sciatic nerves of mice. Each dot stained by LFB represents a nerve fiber. (D-F) Serum liver enzyme levels post-treatment: ALT (D), AST (E), and γ-GT (F). The dashed lines indicate normal reference ranges (n = 6-8). (G) Quantification of nerve fiber density in the sciatic nerves (n = 5).

The harvested livers were further stained with periodic acid-Schiff (PAS). As depicted in Figure 10B,

a large amount of fat vesicles, characteristic of fatty liver disease, were observed in the untreated db/db

mice; however, treatment with Suba@T-gel or Free Suba resulted in a substantial reduction of fat vesicles. Meanwhile, the deeper glycogen-specific staining in the treated mice indicated a marked restoration of hepatic glycogen storage capacity. Additionally, the levels of alanine aminotransferase (ALT), aspartate aminotransferase (AST) and γ -glutamyl transpeptidase (γ -GT) returned to the normal ranges or were comparable to those of wild-type mice (WT) following the administration of Suba@T-gel or Free Suba (Figure 10D-F), indicating the recovery of liver function.

The development of diabetes is also recognized to cause neuropathy, which affects up to 50% of individuals with T2DM [67], and is strongly associated with conditions such as diabetic foot and dementia [68, 69]. Consequently, the sciatic nerves of db/db mice were collected and then stained with Luxol Fast Blue (LFB). As shown in Figure 10C, the sciatic nerve fibers in the placebo group were loosely packed. However, after treatment with Suba@T-gel or Free Suba, the nerve fibers regained a compact arrangement. Meanwhile, a higher density of nerve fibers was observed in the Suba@T-gel and Free Suba groups, as presented in Figure 10G. These results suggest that the administration of Suba@T-gel can slow or even reverse diabetic neuropathy.

Last but not least, no significant differences were observed in other major organs among the different treatment groups, including organ mass, gross morphology (Figure 10A), and histological examination (Figure S16). These outcomes suggest that the db/db mouse model used in this study may not be advanced enough to develop complications in these organs, and that treatment with Suba@T-gel did not cause any tissue abnormalities.

Discussion

Chronic diseases such as diabetes, for which no definitive cure currently exists, represent a significant challenge in modern medicine. The requirement for frequent medication administration often leads to suboptimal patient adherence, further complicating disease management [5, 70]. For example, poor medication adherence in T2MD is associated with inadequate blood sugar control, higher medical costs and significantly increased mortality rates [5]. Over the last two decades, the emergence of GLP-1RAs has notably improved the quality of living and longevity for individuals with diabetes [7, 9, 29]. However, challenges related to medication adherence continue to persist, particularly due to the need for frequent injections [4, 5].

To addressing adherence issues, we exploited a sustained-release system of Suba, spotlighting its

potential for long-acting glycemic control. This system achieved effective glycemic control and comprehensive management of diabetes-related complications for over three weeks in various animal models after just a single injection, thereby developing a promising treatment option for diabetes management.

Injectable and thermosensitive hydrogels composed of PLGA-PEG-PLGA copolymers were selected as the carrier for Suba delivery. This choice was based on the consideration that both PEG and PLGA components have approved by the Food and Drug Administration (FDA) for in vivo use [71], and the biosafety of PLGA-PEG-PLGA hydrogels has also been confirmed in clinical trials [48, 49]. Additionally, the synthesis of PLGA-PEG-PLGA copolymers is straightforward and can be accomplished through a one-step bulk polymerization without the use of organic solvents, and the subsequent purification process is conducted in water, which further enhances their safety and practicability. The PEG/PLGA ratio determine the $T_{\rm gel}$ of the resulting PLGA-PEG-PLGA hydrogel and even influence the formation of a temperature-responsive hydrogel (Figure 2C-D), while the ratio of LA to GA significantly impacted the degradation rate of the hydrogel in vivo (Figure 3B). The thermosensitive hydrogel composed of Copolymer-II (T-gel) was employed for the sustained delivery of Suba due to its suitable T_{gel} and in vivo retention time. The biocompatibility of Copolymer-II and corresponding T-gel were substantiated by in vitro and in vivo biological experiments (Figure 3 and S3-S5).

It should be noted that previous studies have explored the delivery of GLP-1RAs PLGA-PEG-PLGA hydrogels, such as exenatide and lixisenatide [55, 60]. However, these formulations faced notable challenges. Due to the weak interactions between the drug and the carrier polymer, exenatide exhibited a severe burst release (over 40%) on the first day [55]. In contrast, the strong interactions between the drug and the carrier polymer led to a significant incomplete release of lixisenatide (cumulative release amount < 60%) at the late stage [60]. In the present study, these challenges were successfully addressed by leveraging Suba's larger molecular size and its co-assembly moderate interactions with PLGA-PEG-PLGA. This ensured steady, degradation-dependent release profile for up to 60 days in vitro (Figure 4F) and for 3 weeks in vivo (Figure 6). It should be noted that the differences between the in vitro and in vivo release profiles are mainly due to the complex physiological environment in the body, which accelerates the in vivo degradation of the carrier hydrogel [72]. Additionally, T-gel was nearly fully degraded within two weeks following the complete release of Suba *in vivo* (Figure 3B), reducing concerns about polymer accumulation at the injection site and facilitating subsequent injections. These results highlight the advantages of the Suba@T-gel system, extending the duration of GLP-1RA therapy while minimizing undesired fluctuations in drug concentration.

To validate the *in vivo* therapeutic efficacy of Suba@T-gel, we adopted three distinct mouse models: the normal ICR mouse model, the T2DM db/db mouse model and the STZ-induced islet-damaged mouse model, with consistent outcomes observed. Particularly, in the db/db mouse model, the fasting blood glucose levels of mice that received a single injection of Suba@T-gel remained at a normal level until Day 21, while OGTTs demonstrated that the postprandial blood glucose levels were maintained within a healthy range even towards the end of the single dose of Suba@T-gel (Figure S13). HbA_{1c} is the gold standard for assessing long-term blood sugar control [60]. Compared to the placebo group, a single injection of Suba@T-gel plus its subsequently sustained release significantly reduced HbA_{1c} levels, markedly enhanced insulin secretion, and suppressed glucagon release in db/db mice (Figure 7D-H). These positive outcomes were not inferior to those achieved in the Free Suba group but with a drastically reduced injection frequency (7 injections vs. 1 injection).

Beyond glycemic control, diabetes is closely associated with β -cell apoptosis, which contributes to disease progression [73]. Therefore, alleviating or even reversing β -cell apoptosis is essential for effective diabetes treatment [74]. In the STZ-induced islet-damaged mouse model, we found that treatment with Suba@T-gel, compared to a single injection of Free Suba, not only effectively prevented β -cell apoptosis but also remarkably promoted β-cell superior effect proliferation. This the sustained-release formulation is primarily attributed to its prolonged duration of action and enhanced bioavailability.

Diabetes is closely associated with lipid accumulation and ectopic storage [75], which can cause many lipid-related diseases such as obesity, atherosclerosis and fatty liver disease [2, 75, 76]. A single injection of Suba@T-gel treatment effectively mitigated muscle loss and fat accumulation in db/db mice, thereby inhibiting their body weight gain. Despite no changes in FFA levels, significant reductions in TG and TC levels were witnessed following Suba@T-gel treatment, indicating the improvement of overall lipid metabolism (Figure 9C-E). Meanwhile, the treatment of Suba@T-gel

elevated HDL-C levels while lowering LDL-C levels, although no significant differences were detected when compared with the placebo group (Figure 9F-G). We conjecture that these benefits would be further amplified with multiple injections of Suba@T-gel. Furthermore, we found that obese db/db mice had developed fatty liver disease. Intriguingly, treatment with Suba@T-gel markedly reduced the weight of liver, improved the liver function and restore the hepatic glycogen storage capacity in db/db mice. Additionally, the sustained release of Suba provided protective effects on the sciatic nerves of db/db mice, suggesting a potential role in delaying or reversing neuropathic complications. These favorable results highlight that, in addition to long-acting blood sugar control, Suba@T-gel holds the potential to delay or even reverse the development of various diabetes-related complications.

Additionally, rodents such as rats and mice have considerably faster metabolic rates in comparison to humans. Consequently, drugs administered to rats or mice often have significantly shorter $t_{1/2}$ than those achieved in humans [29, 77]. For instance, the $t_{1/2}$ of Suba solution in rats is approximately 24 h, while in humans it can be extended to over a hundred hours [18, 27]. The pharmacokinetic results demonstrated that a single administration of Suba@T-gel could maintain effective plasma Suba concentrations for over 22 days (Figure 6). Based on prior research regarding the extrapolation of subcutaneous hydrogel depot release durations across different species [29], we speculate that a single injection of Suba@Tgel is likely to provide effective glycemic control for far more than three weeks in human patients.

Nevertheless, this study has certain limitations and further investigation is required. One major limitation is that the system has not yet been tested in larger animal models. The study exclusively utilized rat and mouse models. While these models are widely accepted in diabetes research, their metabolic rates and pathophysiology differ significantly from those of humans. Meanwhile, extrapolating the three-week efficacy in mice to a "monthly" human regimen relies on assumptions based on metabolic scaling. Consequently, pharmacokinetic studies in higher species are critical for evaluating the translational potential and scalability of this therapy system.

Conclusion

In this study, we successfully developed an injectable hydrogel-based Suba delivery system that significantly reduced injection frequency without compromising efficacy. The moderate co-assembly interactions between Suba and the carrier polymers plus the large molecular size of Suba ensured the

continuous and slow release of Suba. In a T2DM mouse model, this system achieved sustained glycemic control for three weeks while effectively managing diabetes-related complications. Given its robust efficacy in preclinical models, this system holds promise for treating T2DM and significant improving patient compliance.

Materials and Methods

Animals

Male animals were selected to eliminate the potential interference of sex hormones with the results. For OGTTs, 7-week-old ICR mice were used, while 10-week-old ICR mice were employed for the gel degradation experiment. C57BL/6J mice and db/db mice were 8 weeks old at the start of the experiments. SD rats weighing approximately 500 g were used for pharmacokinetic studies. All rodents had free access to food and water when not undergoing testing and were raised in an environment with a 12-hour day/night cycle. The feeding, anaesthesia, surgical procedures, and handling of experimental animals adhered to the guidelines established by the Experimental Animal Ethics Committee of Fudan University (202101006S).

Materials

PEG1500, tin(II) 2-ethylhexanoate (Sn(Oct)₂) and Pluronic F127 were purchased from Sigma-Aldrich® (St. Louis, MO, USA). Glycolide and D,L-lactide were obtained from Hangzhou Medzone Biotech Ltd. (Hangzhou, China). PVA was acquired from Aladin® (Shanghai, China). Suba was kindly provided by Innogen Pharmaceutical Technology Co., Ltd. (Shanghai, China). Other chemicals and solvents were purchased from Sinopharm Chemical Reagent Co., Ltd. (Shanghai, China) and used as received without further purification.

CCK-8 kit was purchased from Beyotime Biotechnology (Cat# C0048). Ultra-sensitive mouse insulin ELISA kit and mouse GLP-1 ELISA kit were acquired from Crystalchem (Elk Grove Village, IL, USA; Cat# 90080 and 81508, respectively). TG, TC, HDL-C, LDL-C, and HbA_{1c} assay kits were obtained from Nanjing Jiancheng Bioengineering Institute.

Synthesis of PLGA-PEG-PLGA copolymers

PLGA-PEG-PLGA triblock copolymers with varying MWs and LA/GA ratios were synthesized by the ring-opening copolymerization of glycolide and D,L-lactide. Sn(Oct)₂ was selected as the catalyst, while PEG1500 served as the macroinitiator. In brief, a certain amount of PEG was transferred into a three-necked flask and dehydrated under vacuum at

approximately 120 °C for no less than 1 h. Subsequently, after cooling the flask to 80 °C, the appropriate amounts of glycolide, D,L-lactide and Sn(Oct)₂ were introduced into the reaction system. Following purging the flask with argon, the reaction was conducted at 150 °C for 12 h. Thereafter, the crude polymers were washed with 80 °C deionized water at least three times to remove residual monomers and low MW byproducts. Upon lyophilization, the final product was gathered and stored for subsequent use.

Characterization of copolymers

A 400 MHz 1 H-NMR spectrometer (Bruker, AVANCE III HD) was used to confirm the chemical structures and MWs of the resulting copolymers. CDCl₃ was used as the solvent and measurements were conducted at 25 °C. A GPC system (Agilent, 1260) was employed to determine the MWs and $D_{\rm M}$ values of the samples.

Preparation of aqueous copolymer solutions

A predetermined amount of copolymer was weighed and transferred into a glass sample vial, followed by the addition of phosphate-buffered saline (PBS). The resulting mixture was stirred using a magnetic stirrer for 4 days. The pH was then measured and adjusted to 7.4.

Phase diagram

A series of aqueous copolymer solutions with different concentrations were prepared and subsequently transferred into 2-mL tubules for incubation in a water bath. The temperature of the water bath was incrementally increased from 25 °C to 60 °C, with increments of 0.5 °C at each step. After a 10-min equilibrium at each temperature, the tubules containing the samples were inverted in the water bath. No visible flow was observed within 30 s, which was interpreted as a gel. Experiments were repeated three times per sample.

In vivo hydrogel degradation

ICR mice were anesthetized with isoflurane gas, and then 0.2 mL of 25 wt% aqueous solutions of Copolymer-II, IV and V were injected subcutaneously into both sides of the mice's backs. At predetermined time points, some mice were sacrificed for anatomical observation. Subsequently, the optical images of residual hydrogels were captured, and the mass of these residual hydrogels was measured. After lyophilization of these residual hydrogels, the corresponding ¹H NMR spectra were obtained. Additionally, tissue samples containing the remaining hydrogels were harvested for histological analysis.

Rheological study

The temperature-dependent rheological behaviors of aqueous polymer solutions with or without drugs were investigated using a rotational rheometer (Malvern, Kinexus Pro) equipped with a cone plate (cone angle: 1°, diameter: 60 mm, gap: 0.03 mm). Temperature sweep measurements were conducted at a heating rate of 0.5 °C/min over the range of 15 to 45 °C with an oscillation frequency of 10 rad/s.

TEM observation

A 1 wt% aqueous solution of Copolymer-II with or without Suba was dropped onto the copper meshes. The copper meshes were then placed at room temperature or in a 37 °C air bath overnight. After that, the copper webs were scanned via TEM (FEI, Tecnai G2 20 TWIN).

CD measurement

A CD spectrometer (Bruker, BIO-logic MOS-450) was used to analyze the secondary structure of samples. CD measurements were conducted at 25 °C over a wavelength range of 200 to 260 nm or 200 to 350 nm. Each spectrum was corrected by subtracting the corresponding ultra-pure water signal as the baseline and the gas signal in the cavity as the background.

Preparation of Suba-loaded hydrogels

For Suba@T-gel, lyophilized Suba powder was added to a 25 wt% aqueous solution of Copolymer-II at an indicated concentration, and the mixture was then stirred magnetically for 24 h until a homogeneous state was achieved.

For Suba@F127-gel, Pluronic F127 was dissolved in PBS to obtain a 20 wt% solution, after which lyophilized Suba powder was incorporated at a concentration of 2.5 mg/mL and then stirred magnetically for 24 h until uniform.

For Suba@PVA-gel, PVA was dissolved in PBS to prepare a 10 wt% solution and Suba was then added at a concentration of 2.5 mg/mL. Next, the system underwent a freeze-thaw cycle consisting of storage at -20 °C for 6 h and subsequent thawing at room temperature for another 6 h.

In vitro drug release

1 mL of Suba@T-gel, Suba@PVA-gel or Suba@F127-gel was introduced into 10-mL release tubes, respectively. The concentration of Suba in each gel was 2.5 mg/mL. Then, the tubes were placed in a water bath shaker (50 rpm) at 37 °C for an equilibration of 10 min. Next, 8 mL of pre-heated PBS

solution containing 0.025% NaN₃ was added as the release medium. At each sampling time point, optical images of the hydrogels were taken and 5 ml of the release medium was withdrawn and replaced with an equal volume of fresh PBS. All collected samples were stored at -20 °C until analysis. After completion of the release experiment, the concentration of Suba in the collected media was quantified using Mouse GLP-1 ELISA kit.

Fluorescence imaging in mice

RB-modified Copolymer-II was co-dissolved with Copolymer-II in water at a ratio of 1:10,000 to obtain a 25 wt% aqueous polymer solution (RB-gel). Meanwhile, 2.5 µg of Cy7.5-Suba were added to Suba@T-gel, resulting in the formation Cy7.5-Suba@T-gel. Subsequently, 0.2 mL of RB-gel was injected subcutaneously into the right dorsal region of mice, while the same volume of Cy7.5-Suba@T-gel was injected into the left region. Changes in fluorescence intensity at the injection site over time were tracked using a multi-angle small animal optical in vivo imaging system (Biolight Biotechnology Co., Ltd., Aniview Pro). Fluorescence imaging for RB-gel was performed at an excitation wavelength of 560 nm and an emission wavelength of 600 nm, while fluorescence imaging for Cy7.5-Suba utilized an excitation wavelength of 790 nm and an emission wavelength of 810 nm. Each imaging exposure lasted for 1.5 s. The three sets of images were then merged and processed using different pseudocolors.

MRI in mice

T-gel and Suba@T-gel (0.2 mL each) were subcutaneously injected into the right and left dorsal regions of ICR mice, respectively. At designated sampling time points, the residual hydrogels were imaged using a 7.0T high-field small animal MRI system (SHCG, NOVILA 7.0T). T_2 -weighted spin-echo sequences were employed for imaging, with the mouse bladder serving as the reference for localization while capturing both transverse and sagittal views.

OGTT model

Before the measurements, the mice were fasted for 6 h with free access to water. Following the administration of a glucose solution in mice via gavage at a dose of 1 g/kg, blood samples were collected using the tail clipping method at 0, 30, 60, and 120 min post-administration. Subsequently, blood glucose levels were determined by a standard glucose meter.

Pharmacokinetic study

SD rats were randomly assigned into three groups (n = 3 per group): intravenous injection of Suba solution (Free Suba (i.v.)), subcutaneous administration of Suba solution (Free Suba (s.c.)), and subcutaneous injection of Suba@T-gel (Suba@T-gel). The dosage of Suba was set at 2.5 mg/mL, with each rat receiving a single injection (0.5 mL). At specific time points, approximately 0.5 mL of whole blood was collected via the tail vein into anticoagulant tubes. Blood samples were centrifuged at 1000 × g for 10 min at 4 °C, after which the upper plasma layer was collected and stored at -80 °C until analysis. Finally, the concentration of Suba in the plasma was quantified using a Mouse GLP-1 ELISA kit.

Diabetic db/db mouse model

Diabetic db/db mice aged 8 weeks were randomly divided into three groups (eight per group): Placebo (subcutaneous injection of 0.2 mL normal saline every three days), Free Suba (subcutaneous injection of 0.2 mL Suba solution at a concentration of 0.357 mg/mL every three days) and Suba@T-gel (a single subcutaneous injection of 0.2 mL Suba@T-gel (2.5 mg/mL)). The mice in the Placebo and Free Suba groups received a total of seven injections. Meanwhile, another group consisting of eight normal C57 mice with the same age was designated as WT and did not receive any administration. During the 22-day experimental period, the mice had free access to food and water on even days, while they underwent overnight fasting on odd days. Random blood glucose levels were measured on even days, while fasting blood glucose levels were assessed on odd days. Additionally, changes in the body weight of mice were monitored throughout the study period.

Before and after the treatment period, body composition analysis was performed using a Bruker minispec LF50 body composition analyzer to measure fat and lean mass proportions, which were normalized relative to body weight. On Day 22 of the experiment, whole blood (0.5 mL) was collected from each mouse into heparinized anticoagulant tubes or serum-separating tubes. After centrifugation (1000 g, 10 min, 4 °C), the serum and plasma were collected and stored for subsequent biochemical analyses.

Tissue collection was made following euthanasia, the heart, liver, spleen, lungs, kidneys, pancreas, and sciatic nerve were harvested, fixed in 10% neutral-buffered formalin, and processed for histological analysis. Serum levels of insulin, TG, TC, FFA, HDL-C, LDL-C, ALT, AST and γ -GT were quantified according to the manufacturer's instructions for the respective assay kits. For HbA_{1c}

determination, 5 μ L of whole blood was added to a sterile centrifuge tube and subsequently 60 μ L of lysis buffer was added. The mixture was incubated at room temperature for 10 min to ensure complete lysis of the red blood cells. Following this, HbA_{1c} levels was determined using the colorimetric reaction of horseradish peroxidase according to the kit protocol.

Sections of the collected tissue specimens were obtained through a series of processes including dehydration, clearing, embedding, and sectioning. The heart, spleen, lungs, and kidneys were stained with H&E. The livers were stained with PAS, while the sciatic nerves were stained with LFB. The pancreas underwent immunohistochemical staining for insulin and glucagon. Using Image J, the area of insulin-positive signals was extracted; the insulin signal was quantified using intensity-weighted measurements and then normalized to the Placebo group. Similarly, Image J was used to extract glucagon-positive cells and calculate the proportion of alpha cells within the islets while normalizing these values to the Placebo group.

Islet injury model

An islet injury model was established using multiple small-dose STZ (Beyotime) administrations, with placebo treatment serving as the control group. Specifically, a fresh 1 wt% STZ solution was prepared in a citrate/citrate buffer under light-protected conditions. After a 6-hour fasting period, C57 mice were intraperitoneally injected with STZ at a dose of 40 mg/kg. This procedure was repeated for five consecutive days, during which random blood glucose levels were monitored daily. Four weeks post-induction, the diabetic C57 mice were divided into three groups: the STZ control group (n = 8), which received placebo treatment after β -cell injury induction; the STZ + Suba@T-gel group, which received a single subcutaneous injection Suba@T-gel (2.5 mg/mL, 0.2 mL, n = 8) and the STZ + Free Suba group, which received a single subcutaneous injection of Free Suba (2.5 mg/mL, 0.2 mL, n = 8). Next, blood glucose levels were continuously monitored for subsequent four weeks, after which an OGTT was conducted. Following this, the mice were euthanized and their pancreases were gathered. Finally, the pancreatic samples were sectioned and subjected to Ki67 and TUNEL immunofluorescent staining. The insulin-positive regions, Ki67-positive cells and total pancreatic areas were quantified using ImageJ software. The percentage of Ki67-positive cells was obtained by counting the ratio of Ki67-positive β cells to the total number of β cells. β -cell mass was determined by multiplying the ratio of insulin-positive area to total

pancreatic area by the pancreatic weight.

Statistical analysis

All data were expressed as mean \pm standard deviation. Two-tailed Student's t-test was performed to analyze the statistical significance between two groups. We used "*" when p < 0.05, "**" when p < 0.01 and "***" when p < 0.001.

Abbreviations

IDF: International Diabetes Federation; T2DM: Type 2 diabetes mellitus; GLP-1: Glucagon-like peptide-1; DPP-4: Dipeptidyl peptidase-4; GLP-1RA: Glucagon-like peptide-1 receptor agonist; HbA_{1c}: Glycated hemoglobin; PEG: Poly(ethylene glycol); PLGA: Poly(lactic acid-co-glycolic acid); LA: lactic acid; GA: glycolic acid; GPC: Gel permeation chromatography; ¹H-NMR: Proton nuclear magnetic resonance; TEM: Transmission electron microscopy; CD: Circular dichroism; DLS: Dynamic light scattering; CMC: Critical micelle concentration; PVA: Poly(vinyl alcohol); CCK-8: Cell Counting Kit-8; H&E: Hematoxylin and eosin; MRI: Magnetic resonance imaging; RB: Rhodamine B; AUC: Area under the curve; ICR: Institute of Cancer Research; OGTT: Oral glucose tolerance test; SD: Sprague-Dawley; STZ: Streptozotocin; TUNEL: Terminal deoxynucleotidyl transferase dUTP nick end labeling; TG: Triglyceride; TC: Total cholesterol; FFA: Free fatty acid; HDL-C: LDL-C: High-density lipoprotein cholesterol; Low-density lipoprotein cholesterol; PAS: Periodic acid-Schiff; LFB: Luxol Fast Blue; ALT: Alanine aminotransferase; AST: Aspartate aminotransferase; γ-GT: Gamma-glutamyl transferase; WT: Wild-type; FDA: Food and Drug Administration; PBS: Phosphate-buffered saline; ELISA: Enzyme-linked immunosorbent assay.

Supplementary Material

Supplementary methods and figures. https://www.thno.org/v16p1833s1.pdf

Acknowledgements

Funding

This work was funded by the National Natural Science Foundation of China (grant no. 22475052), the Natural Science Foundation of Shanghai (grant no. 23ZR1406800), and Special Project for Emerging Interdisciplinary Research in the Health Industry of the Shanghai Municipal Health Commission (grant no. 2022JC030). The schematic illustrations were created with BioRender.com.

Data availability

All data supporting the findings of this study are available within the article and its supplementary files. Any additional reasonable requests for information can be directed to the corresponding authors.

Author contributions

Conceptualization: H.C. Wang, Q.H. Wang and L. Yu

Methodology: H.C. Wang, L. Yu

Investigation: H.C. Wang, Z.Y. Chen, S.Y. Gu,

Y.B. Wang, Y. Wang, C.Y. Gao and L. Yu

Visualization: H.C. Wang and J.Y. Shi

Funding acquisition: L. Yu

Project administration: J.D. Ding, Q.H. Wang. and L. Yu

Supervision: J.D. Ding, Q.H. Wang and L. Yu Writing – original draft: H.C. Wang

Writing – review & editing: H.C. Wang, Z.Y. Chen, Y. Wang, J.D. Ding, Q.H. Wang and L. Yu

Competing Interests

QH. Wang is a shareholder of Innogen Pharmaceutical Technology Co., Ltd. Other authors declare that they have no known competing financial interests or personal relationships that could have appeared to influence the work reported in this paper.

References

- [Internet] International Diabetes Federation Diabetes Atlas (11th edition). 2025. https://www.diabetesatlas.org/.
- Wong ND, Sattar N. Cardiovascular risk in diabetes mellitus: epidemiology, assessment and prevention. Nat Rev Cardiol. 2023; 20: 685-95.
- Xu DH, Zhang XY, Liu SY, Wei J, Zhan JH, Du JK, et al. KLK8/HGF/Met signaling pathway mediates diabetes-associated hippocampal neuroinflammation in male mice. Theranostics. 2025; 15: 6290-312.
- Ahmad E, Lim S, Lamptey R, Webb DR, Davies MJ. Type 2 diabetes. Lancet. 2022; 400: 1803-20.
- Polonsky WH, Henry RR. Poor medication adherence in type 2 diabetes: recognizing the scope of the problem and its key contributors. Patient Prefer Adherence. 2016; 10: 1299-307.
- Kreymann B, Ghatei MA, Williams G, Bloom SR. Glucagon-like peptide-1 7-36: A physiological incretin in man. Lancet. 1987; 2: 1300-4.
- Drucker DJ. Mechanisms of Action and Therapeutic Application of Glucagon-like Peptide-1. Cell Metab. 2018; 27: 740-56.
- Cary BP, Hager MV, Mariam Z, Morris RK, Belousoff MJ, Deganutti G, et al. Prolonged signaling of backbone-modified glucagon-like peptide-1 analogues with diverse receptor trafficking. Proc Natl Acad Sci U S A. 2025; 122: e2407574122.
- Drucker DJ. Expanding applications of therapies based on GLP1. Nat Rev Endocrinol. 2025; 21: 65-6.
- Drucker DJ. The benefits of GLP-1 drugs beyond obesity. Science. 2024; 385: 258-60
- Chuong V, Farokhnia M, Khom S, Pince CL, Elvig SK, Vlkolinsky R, et al. The glucagon-like peptide-1 (GLP-1) analogue semaglutide reduces alcohol drinking and modulates central GABA neurotransmission. JCI Insight. 2023; 8: 170671.
- 12. Feng JN, Jin TR. Hepatic function of glucagon-like peptide-1 and its based diabetes drugs. Med Rev. 2024; 4: 312-25.
- Pang J, Feng JN, Ling WH, Jin TR. The anti-inflammatory feature of glucagon-like peptide-1 and its based diabetes drugs—therapeutic potential exploration in lung injury. Acta Pharm Sin B. 2022; 12: 4040-55.
- Ghosh P, Fontanella RA, Scisciola L, Pesapane A, Taktaz F, Franzese M, et al. Targeting redox imbalance in neurodegeneration: characterizing the role of GLP-1 receptor agonists. Theranostics. 2023; 13: 4872-84.

- Drucker DJ, Nauck MA. The incretin system: glucagon-like peptide-1 receptor agonists and dipeptidyl peptidase-4 inhibitors in type 2 diabetes. Lancet. 2006; 368: 1696-705.
- Yao HQ, Zhang AQ, Li DL, Wu YQ, Wang C, Wan J, et al. Comparative effectiveness of GLP-1 receptor agonists on glycaemic control, body weight, and lipid profile for type 2 diabetes: systematic review and network meta-analysis. BMJ. 2024; 384: e076410.
- Kimura T, Katakura Y, Shimoda M, Kawasaki F, Yamabe M, Tatsumi F, et al. GLP-1 Receptor Agonists Dulaglutide and Semaglutide in Japanese Patients with Type 2 Diabetes-Randomized, Parallel-Group, Multicenter, Open-Label Trial. Diabetes. 2023; 72 (Suppl 1): 748-P.
- Liao YJ, Ma AR, Wang ZH, Zhou Y, Liu L, Zhang N, et al. Pharmacokinetic and pharmacodynamic studies of supaglutide in rats and monkeys. Eur J Pharm Sci. 2022; 175: 106218.
- Overgaard RV, Hertz CL, Ingwersen SH, Navarria A, Drucker DJ. Levels of circulating semaglutide determine reductions in HbA1c and body weight in people with type 2 diabetes. Cell Rep Med. 2021; 2: 100387.
- American Diabetes Association Professional Practice Committee. 9.
 Pharmacologic Approaches to Glycemic Treatment: Standards of Care in Diabetes-2024. Diabetes Care. 2024; 47 (Suppl 1): S158-S78.
- Gao ZJ, Wei Y, Ge J, Liu JX, Qin Y, Gong FL, et al. Development of 1 Month Sustained-Release Microspheres Containing Liraglutide for Type 2 Diabetes Treatment. ACS Appl Mater Interfaces. 2024; 16: 25869-78.
- Park JK, Piao ZY, Lee HJ, Jeong B. Poly(L-threonine-co-l-threonine Succinate) Thermogels for Sustained Release of Lixisenatide. Biomacromolecules. 2024; 25: 4946-55.
- Yu L, Li K, Liu XJ, Chen C, Bao YC, Ci TY, et al. *In Vitro* and *In Vivo* Evaluation
 of a Once-weekly Formulation of an Antidiabetic Peptide Drug Exenatide in
 an Injectable Thermogel. J Pharm Sci. 2013; 102: 4140-9.
- Gao XL, Di YJ, Lv Y, Luan YC, Xiong Y, Xu YL, et al. A pharmacokinetic study comparing the biosimilar HEC14028 and Dulaglutide (Trulicity®) in healthy Chinese subjects. Clin Transl Sci. 2024; 17: e13775.
- Wang QH, Chen K, Liu R, Zhao F, Gupta S, Zhang NN, et al. Novel GLP-1 Fusion Chimera as Potent Long Acting GLP-1 Receptor Agonist. PLoS ONE. 2010: 5: e12734.
- Ren LW, Cui QL, Liu WJ, Wang LQ, Liao YJ, Feng Y, et al. Novel GLP-1
 Analog Supaglutide Stimulates Insulin Secretion in Mouse and Human Islet
 Beta-Cells and Improves Glucose Homeostasis in Diabetic Mice. Front Physiol.
 2019; 10: 930.
- Zhou Y, Jiang X, Lou Y, Ma AR, Li J, Zhao Y, et al. Safety, PK, PD, and Efficacy
 of Weekly Dosing Supaglutide in Patients with T2D. Diabetes. 2022; 71 (Suppl
 1): 88-J B
- Wang QH, Zhou Y, Wang WM, Tong GY, Jia WN, Li L, et al. Efficacy and Safety of Supaglutide Monotherapy in Patients with Type 2 Diabetes. Diabetes. 2023; 72 (Suppl 1): 757-P.
- d'Aquino AI, Maikawa CL, Nguyen LT, Lu K, Hall IA, Jons CK, et al. Use of a biomimetic hydrogel depot technology for sustained delivery of GLP-1 receptor agonists reduces burden of diabetes management. Cell Rep Med. 2023; 4: 101292.
- Gao ZJ, Wei Y, Ma GH. A review of recent research and development on GLP-1 receptor agonists-sustained-release microspheres. J Mater Chem B. 2023; 11: 11184-97.
- Zhou YH, Chen ZX, Zhao D, Li D, He CL, Chen XS. A pH-Triggered Self-Unpacking Capsule Containing Zwitterionic Hydrogel-Coated MOF Nanoparticles for Efficient Oral Exendin-4 Delivery. Adv Mater. 2021; 33: 2102044.
- Chen XB, Wang HC, Shi JY, Chen ZY, Wang YB, Gu SY, et al. An injectable and active hydrogel induces mutually enhanced mild magnetic hyperthermia and ferroptosis. Biomaterials. 2023; 298: 122139.
- Cao DLG, Ding JD. Recent advances in regenerative biomaterials. Regen Biomater. 2022; 9: rbac098.
- Wang L, Jiang Y, Yao YL, Deng YD, Liu ZQ, Ding JT, et al. Injectable drug-loaded thermosensitive hydrogel delivery system for protecting retina ganglion cells in traumatic optic neuropathy. Regen Biomater. 2024; 11: rbae124.
- Cheng Y, Huangfu YN, Zhao TY, Wang LX, Yang J, Liu J, et al. Thermosensitive hydrogel with programmed dual-octenidine release combating biofilm for the treatment of apical periodontitis. Regen Biomater. 2024; 11: rbae031.
- Zhou H, He ZY, Cao YD, Chu L, Liang B, Yu KX, et al. An injectable magnesium-loaded hydrogel releases hydrogen to promote osteoporotic bone repair via ROS scavenging and immunomodulation. Theranostics. 2024; 14: 3739-59.
- Deng JJ, Wang X, Zhang WH, Sun LY, Han XX, Tong XQ, et al. Versatile hypoxic extracellular vesicles laden in an injectable and bioactive hydrogel for accelerated bone regeneration. Adv Funct Mater. 2023; 33: 2211664.
- Zhao D, Rong Y, Li D, He CL, Chen XS. Thermo-induced physically crosslinked polypeptide-based block copolymer hydrogels for biomedical applications. Regen Biomater. 2023; 10: rbad039.
- Woo Y, Patel M, Kim H, Park JK, Jung YJ, Cha SS, et al. Pralatrexate Sustainably Released from Polypeptide Thermogel Is Effective for Chondrogenic Differentiation of Mesenchymal Stem Cells. ACS Appl Mater Interfaces. 2022; 14: 3773-83.

- Ding JF, Wang TR, Lin ZQ, Li ZY, Yang JX, Li FJ, et al. Chiral polypeptide hydrogels regulating local immune microenvironment and anti-tumor immune response. Nat Commun. 2025; 16: 1222.
- Seo BB, Park MR, Song SC. Sustained Release of Exendin 4 Using Injectable and Ionic-Nano-Complex Forming Polymer Hydrogel System for Long-Term Treatment of Type 2 Diabetes Mellitus. ACS Appl Mater Interfaces. 2019; 11: 15201-11
- Hong LTA, Kim YM, Park HH, Hwang DH, Cui YX, Lee EM, et al. An injectable hydrogel enhances tissue repair after spinal cord injury by promoting extracellular matrix remodeling. Nat Commun. 2017; 8: 533.
- Han B, Fujii S, van der Vlies AJ, Ghasemi M, Del Mundo JT, Kiemle SN, et al. Thermally Induced Gelling Systems Based on Patchy Polymeric Micelles. Adv Funct Mater. 2024: 2417544.
- Kim J, Francis DM, Sestito LF, Archer PA, Manspeaker MP, O'Melia MJ, et al. Thermosensitive hydrogel releasing nitric oxide donor and anti-CTLA-4 micelles for anti-tumor immunotherapy. Nat Commun. 2022; 13: 1479.
- Rouco H, Permuy M, Munoz F, Vazquez JA, Caeiro JR, Landin M, et al. Micelle into gel thermosensitive intra-articular hydrogels for osteoarthritis management. J Control Release. 2025; 381: 113639.
- Shi JY, Yu L, Ding JD. PEG-based thermosensitive and biodegradable hydrogels. Acta Biomater. 2021; 128: 42-59.
- Chen XB, Wang ML, Yang XW, Wang YB, Yu L, Sun J, et al. Injectable hydrogels for the sustained delivery of a HER2-targeted antibody for preventing local relapse of HER2-tbreast cancer after breast-conserving surgery. Theranostics. 2019; 9: 6080-98.
- 48. DuValla GA, Tarabar D, Seidela RH, Elstad NL, Fowers KD. Phase 2: a dose-escalation study of OncoGel (ReGel/paclitaxel), a controlled-release formulation of paclitaxel, as adjunctive local therapy to external-beam radiation in patients with inoperable esophageal cancer. Anticancer Drugs. 2009; 20: 89-95.
- Vukelja SJ, Anthony SP, Arseneau JC, Berman BS, Cunningham CC, Nemunaitis JJ, et al. Phase 1 study of escalating-dose OncoGel® (ReGel®/paclitaxel) depot injection, a controlled-release formulation of paclitaxel, for local management of superficial solid tumor lesions. Anticancer Drugs. 2007; 18: 283-9.
- Chen XB, Zhang JL, Wu KT, Wu XH, Tang JY, Cui SQ, et al. Visualizing the *in vivo* evolution of an injectable and thermosensitive hydrogel using tri-modal bioimaging. Small Methods. 2020; 4: 2000310.
- Cui SQ, Yu L, Ding JD. Semi-bald Micelles and Corresponding Percolated Micelle Networks of Thermogels. Macromolecules. 2018; 51: 6405-20.
- Yu L, Zhang H, Ding JD. A subtle end-group effect on macroscopic physical gelation of triblock copolymer aqueous solutions. Angew Chem Int Ed. 2006; 45: 2232-5.
- 53. Yu L, Ding JD. Injectable hydrogels as unique biomedical materials. Chem Soc Rev. 2008; 37: 1473-81.
- Wu KT, Chen XB, Gu SY, Cui SQ, Yang XW, Yu L, et al. Decisive Influence of Hydrophobic Side Chains of Polyesters on Thermoinduced Gelation of Triblock Copolymer Aqueous Solutions. Macromolecules. 2021; 54: 7421-33.
- Li K, Yu L, Liu XJ, Chen C, Chen QH, Ding JD. A long-acting formulation of a polypeptide drug exenatide in treatment of diabetes using an injectable block copolymer hydrogel. Biomaterials. 2013; 34: 2834-42.
- Stauffer SR, Peppas NA. POLY(VINYL ALCOHOL) HYDROGELS PREPARED BY FREEZING-THAWING CYCLIC PROCESSING. Polymer. 1992; 33: 3932-6.
- Adelnia H, Ensandoost R, Moonshi SS, Gavgani JN, Vasafi EI, Ta HT. Freeze/thawed polyvinyl alcohol hydrogels: Present, past and future. Eur Polym J. 2022: 164: 110974.
- Chen YP, Li YZ, Shen WJ, Li K, Yu L, Chen QH, et al. Controlled release of liraglutide using thermogelling polymers in treatment of diabetes. Sci Rep. 2016: 6: 31593.
- Gao JM, Xu X, Yu XY, Fu Y, Zhang HJ, Gu SY, et al. Quantitatively relating magnetic resonance T₁ and T₂ to glycosaminoglycan and collagen concentrations mediated by penetrated contrast agents and biomacromolecule-bound water. Regen Biomater. 2023; 10: rbad035.
- Zhuang YP, Yang XW, Li YM, Chen YP, Peng XC, Yu L, et al. Sustained Release Strategy Designed for Lixisenatide Delivery to Synchronously Treat Diabetes and Associated Complications. ACS Appl Mater Interfaces. 2019; 11: 20404-18
- 61. Arai T, Hayashi E, Maeda S, Matsubara T, Fujii H, Shinohara K, et al. Liver-derived Neuregulin1 α stimulates compensatory pancreatic β cell hyperplasia in insulin resistance. Nat Commun. 2025; 16: 1950.
- Baetens D, Stefan Y, Ravazzola M, Malaisselagae F, Coleman DL, Orci L. Alteration of islet cell-populations in spontaneously diabetic mice. Diabetes. 1978; 27: 1-7.
- Jin TR, Chen YE. International Accolades for GLP-1 Research: Recognizing Pioneers in Diabetes and Obesity Treatment Across Five Prestigious Awards. Cardiovasc Drugs Ther. 2025; 39: 9-12.
- von Eckardstein A, Nordestgaard BG, Remaley AT, Catapano AL. High-density lipoprotein revisited: biological functions and clinical relevance. Eur Heart J. 2023; 44: 1394-407.
- 65. Ference BA, Ginsberg HN, Graham I, Ray KK, Packard CJ, Bruckert E, et al. Low-density lipoproteins cause atherosclerotic cardiovascular disease. 1. Evidence from genetic, epidemiologic, and clinical studies. A consensus statement from the European Atherosclerosis Society Consensus Panel. Eur Heart J. 2017; 38: 2459-72.

- Mukherjee S. Symptoms and Correlations in Newly Diagnosed Type 2 Diabetes Mellitus (T2DM) with Nonalcoholic Fatty Liver Disease (NAFLD). Diabetes. 2024; 73 (Suppl 1): 1593-P.
- 67. Elaíros MA, Andersen H, Bennett DL, Savelieff MG, Viswanathan V, Callaghan BC, et al. Towards prevention of diabetic peripheral neuropathy: clinical presentation, pathogenesis, and new treatments. Lancet Neurol. 2022; 21: 922-36.
- McDermott K, Fang M, Boulton AJM, Selvin E, Hicks CW. Etiology, Epidemiology, and Disparities in the Burden of Diabetic Foot Ulcers. Diabetes Care. 2023; 46: 209-21.
- Biessels GJ, Despa F. Cognitive decline and dementia in diabetes mellitus: mechanisms and clinical implications. Nat Rev Endocrinol. 2018; 14: 591-604.
- Jindal AB, Bhide AR, Salave S, Rana D, Benival D. Long-acting parenteral drug delivery systems for the treatment of chronic diseases. Adv Drug Deliv Rev. 2023: 198: 114862.
- Crabtree AA, Boehnke N, Bates FS, Hackel BJ. Consequences of poly(ethylene oxide) and poloxamer P188 on transcription in healthy and stressed myoblasts. Proc Natl Acad Sci U S A. 2023; 120: e2219885120.
- Yu L, Zhang Z, Zhang H, Ding JD. Biodegradability and biocompatibility of thermoreversible hydrogels formed from mixing a sol and a precipitate of block copolymers in water. Biomacromolecules. 2010; 11: 2169-78.
- Sasaki H, Saisho Y, Inaishi J, Watanabe Y, Tsuchiya T, Makio M, et al. Reduced beta cell number rather than size is a major contributor to beta cell loss in type 2 diabetes. Diabetologia. 2021; 64: 1816-21.
- Karakose E, Wang XD, Wang P, Carcamo S, Demircioglu D, Lambertini L, et al. Cycling alpha cells in regenerative drug-treated human pancreatic islets may serve as key beta cell progenitors. Cell Rep Med. 2024; 5: 101832.
- Carlier A, Phan F, Szpigel A, Hajduch E, Salem J-E, Gautheron J, et al. Dihydroceramides in Triglyceride-Enriched VLDL Are Associated with Nonalcoholic Fatty Liver Disease Severity in Type 2 Diabetes. Cell Rep Med. 2020; 1: 100154.
- Zheng LW, Than A, Zan P, Li DS, Zhang ZY, Leow M, et al. Mild-photothermal and nanocatalytic therapy for obesity and associated diseases. Theranostics. 2024; 14: 5608-20.
- Shinde UP, Joo MK, Moon HJ, Jeong B. Sol-gel transition of PEG-PAF aqueous solution and its application for hGH sustained release. J Mater Chem. 2012; 22: 6072-9.